Master of Science

Analysis of hepatic immune microenvironment using experimental NASH animal model

The Graduate School
of the University of Ulsan
Department of Medical Science

Hee Seon Lim

Analysis of hepatic immune microenvironment using experimental NASH animal model

Supervisor: Woo-Chan Son

A Dissertation

Submitted to
the Graduate School of the University of Ulsan.
In partial Fulfillment of the Requirements
for the Degree of

Master of Science

by

Hee Seon Lim

The Graduate School
of the University of Ulsan
Department of Medical Science
February 2022

Analysis of hepatic immune microenvironment using experimental NASH animal model

This certifies that the master's thesis of Hee Seon Lim is approved.

_____

Committee Chairman Dr. Young Soo Park

_____

Committee Member Dr. Jong Hoa Ok

_____

Committee Member Dr. Woo-Chan Son

The Graduate School
of the University of Ulsan
Department of Medical Science

February 2022

Contents

ABSTRACT

Non-alcoholic steatohepatitis (NASH) is a dangerous disease that can progress to hepatocellular carcinoma (HCC) with an increasing prevalence worldwide. In parallel with this trend, the prevalence of NASH in Korean adult population has also increased. Because there are no approved drugs to treat it, research on NASH is being actively conducted. In particular, the need for research how changes in hepatic microenvironment affect the progression of the disease is increasing.

Considerable effort has been made to understand the role of hepatic immune cells in NASH. However, numerous questions remain. Our goal was to characterize the dynamic changes in immune cells residing in the liver as well as infiltrating from the outside, which were observed at the early stage of NASH using stelic animal model (STAM). Frist, we identified that the activity of monocyte-derived macrophages (MoMFs), which were circulating through the blood, became more pronounced as the non-alcoholic fatty liver disease (NAFLD) progressed. At the same time, we observed the proportion of M2 macrophages in the liver decreased throughout the disease. This was critical information that could indirectly infer that the balance of M1/M2 macrophages was disturbed at the early stage of disease. Next, we confirmed that $CD8^+$ T cells increased proportionally with disease progression.

It is important to use the appropriate animal models that can represent humans in the research of disease. In that sense, the STAM model is a good animal model that can be induced from NAFLD to HCC in a short time period and can reflect clinical stratification in humans as well. Existing studies have presented many research results by inducing NAFLD through diet or chemicals, but these models do not induce HCC in a short time and have limitations in that similarity to humans is low. In this study, changes in hepatic immune microenvironment were first observed using flow cytometry and immunohistochemistry in the STAM model,

which is considered to be most similar to clinical stratification. These results are expected to serve as an important basis for further studies.

Keywords : non-alcoholic fatty liver disease (NAFLD), non-alcoholic steatohepatitis (NASH), hepatocellular carcinoma (HCC), stelic animal model (STAM), Kupffer cell (KC), monocyte-derived macrophage (MoMF)

LIST OF FIGURES AND TABLES

ABBREVIATION

ALT, alanine aminotransferase

APCs, antigen-presenting cells

ASCVD, atherosclerotic cardiovascular disease

AST, aspartate aminotransferase

CCL2, chemokine (C-C motif) ligand 2

CCl4, carbon tetrachloride

CCR2, c-c chemokine receptor type 2

CDAHFD, choline-deficient, L-amino acid-defined high fat diet

CVD, cardiovascular disease

DENA, diethylnitrosamine

DM, diabetes mellitus

DMBA, 9,10-dimethyl-1,2-benzanthracene

EDTA, ethylenediaminetetraacetic acid

FACS, fluorescence-activated cell sorting

FBS, fetal bovine serum

GEMM, genetically engineered mouse models

H&E, hematoxylin and eosin

HCC, hepatocellular carcinoma

HFD, high fat diet

HPF, high power field

HSCs, hepatic stellate cells

IACUC, institutional animal care and use committee

IHC, immunohistochemistry

KCs, Kupffer cells

MCD, methionine/choline deficient

MoMFs, Monocyte-derived macrophages

NAFLD, non-alcoholic fatty liver disease

NAS, non-alcoholic fatty liver disease activity score

NASH, non-alcoholic steatohepatitis

NMOR, N-nitrosomorpholine

PBS, phosphate-buffered saline

PPAR, peroxisome proliferator-activated receptor

RBCs, red blood cells

SD, standard deviation

STAM, stelic animal model

STZ, streptozocin

TG, triglycerides

TNF-α, tumor necrosis factor-α

. INTRODUCTION

Non-alcoholic fatty liver disease (NAFLD), the hepatic manifestation of metabolic syndrome, has emerged as the major liver disease worldwide with no approved therapeutic option currently available [1]. It is a chronic liver disease characterized by excessive cytoplasmic accumulation of triglyceride without a history of alcohol abuse [2]. As a result of the pandemic spread of obesity and type 2 diabetes mellitus (T2DM), NAFLD has become one of the most important cause of liver disease [3]. The global prevalence of NAFLD has been estimated to range from 2.8% to 46% [4]. Although still not fully understood, various causes including genetic factors, environmental factors have contributed to NAFLD [1]. Epidemiological studies are difficult to conduct as no markers that are completely sensitive or specific for the diagnosis of NALFD. Therefore, the current gold standard for diagnosis and staging fatty liver disease is a biopsy [5].

The pathological progression of NAFLD has broad spectrum from simple steatosis, non-alcoholic steatosis (NASH), fibrosis, and to hepatocellular carcinoma (HCC). It is also associated with an increased risk of cardiovascular disease (CVD) and atherosclerotic cardiovascular disease (ASCVD) [6], [7]. While simple steatosis is considered relatively mild disease, NASH is more aggressive type in which significant immune cells infiltrate the liver [8] and is characterized by varying degrees of hepatic inflammation and fibrosis, in addition to hepatic steatosis [9]. HCC could occur as a terminal complication of non-cirrhotic and cirrhotic NASH [10]. Although the risk of HCC on a NASH background was lower than that due to chronic hepatitis C, the high prevalence of NAFLD raised cause for disease [11]. NASH-to-HCC progression relates the accumulation of lipids in the liver, which provoke inflammation and modified immune cell composition [12], [13].

Because NASH is not completely understood, physiologic and pathologic similarity is

essential for animal model to study NASH and associated diseases. Limited understanding of disease mechanisms hindered the development of clinically relevant NASH models and pharmacotherapy. Therefore, various animal models have been established to study the pathophysiology of NASH and the NASH-to-HCC transition, and these can be divided into three main categories: diet-induced model, diet + toxin-induced model and genetic model [14].

Dietary models are most similar in the course of disease development. Diet+toxin induced models quickly lead to metabolic disturbances and severe liver damage, but not without drawbacks. Another liver cancer animal models are genetically engineered mouse models (GEMM), chemotoxic agents induced models, implantation models and humanized mouse models [15], [16], [17]. Various GEMM which manipulates oncogenes or tumor suppressor genes to induce liver cancer have been developed. The target oncogenes include c-Myc, β-Catenin, Ras and myr-Akt, and tumor suppressor gene is p53 [18], [19], [20]. Chemotoxic agents such as CCl4, DENA, NMOR and DMBA are easy to cause liver disease. Many studies about NASH and the NASH-to-HCC transition have often employed animal models mentioned above.

In addition, recent studies have shown that the liver microenvironment may play a critical role in NASH and HCC progression [21]. Because HCC is one of the cancers related with inflammation, chronic inflammatory environment can lead to cancer [22]. Modified immune reactions in NASH with chronic inflammation are also associated with the development of HCC [23].

The liver is a unique immunological site as it is repeatedly exposed to highly immunogenic content draining from the gut. Although the hepatic immunity has various mechanisms, the liver maintains the ability to comprehensive immune responses upon inflammation, such as damaged hepatocytes in NASH, through recruitment of monocytes, granulocytes, and additional lymphocytes. This characteristic requires homeostatic suppression of both immune cells resident in the liver and those in movement through the liver's sinusoids [8]. Therefore,

the liver offers a unique proinflammatory microenvironment that is composed of various immunologically active cells, including Kupffer cells (KCs), T cells, antigen-presenting cells (APCs), and hepatic stellate cells (HSCs). To identify the pathogenic mechanisms of NASH, recent studies have attempted to elucidate the immunological correlation of disease progression and the detailed cellular components, and their interactions.

Many studies have investigated the effects of NASH or NASH-to-HCC immune microenvironments using dietary animal models [24], [25]. Compared with studies that have generated NASH through dietary methods, such as methionine/choline deficient (MCD) diet, high fat diet (HFD), choline-deficient, L-amino acid-defined high fat diet (CDAHFD), the proportion of studies using the diet+toxin model was low. However, the hepatic microenvironment of dietary induced models would be quite different from liver cancer occurred by multi-step process. In this regard, STAM model, diet+toxin induced model, metabolically reproduce development of NASH [26], [27]. We chose the STAM model for this study for this reason. To our knowledge, there is no results of investigating the hepatic immune microenvironment using STAM model. Therefore, we aimed to examine how the liver microenvironment of STAM mice changes with disease progression in early stage of NASH.

The STAM model, which represent patients who develop HCC among NASH populations, is initially designed for investigate HCC [28]. It induces most of the NAFLD spectrum in a short time period and is widely used in research because it is considered to a good animal model to represent human counterpart. Additionally, the STAM mice fulfill criteria for HCC diagnoses and demonstrate the following features : having detectable tumor nodules, an average tumorigenesis rate of 100% from 16 to 20 weeks of age, no visible metastasis, and relatively preserved liver functions [29].

To better understand the pathophysiological changes in NASH and HCC progression, we used STAM mice to identify if the liver microenvironment plays a crucial role in the

pathogenesis of NAFLD, NASH, and HCC. We focused on intrahepatic lymphocyte and macrophage subpopulations that are thought to play an important role in NASH progression.

T cells are involved in NAFLD/NASH pathogenesis, inducing differential effects on adiposity, insulin resistance, steatosis, hepatic inflammation, hepatic injury [30]. However, as the first line of defense against pathogenic condition, the liver must retain a large population of phagocytes that remove foreign materials. Therefore, about 80% of the body's macrophages reside in the liver, including Kupffer cells (KCs) and Monocyte-derived macrophages (MoMFs), both of which play critical roles in the pathogenesis of NASH [8].

Macrophages are a heterogenous population of immune cells and generally consist of two classes: tissue-resident KCs and infiltrating macrophages [31]. Liver resident macrophages, KCs, are derived from macrophage stem cells generated during development in the yolk sac or fetal liver and maintain themselves through adulthood by self-renewal independent from blood-borne monocytes [32]. They constitute approximately 30% of the hepatic sinusoidal cells and their major roles are to uptake and detoxify gut-derived endotoxin and maintain homeostasis against invasion by foreign organisms [33]. In addition, KCs are associated with the production of proinflammatory markers such as TNF-α and IL-1β as well as anti-inflammatory markers including IL-10 and arginase [34]. They are often characterized by high F4/80 surface expression and are negative for chemokine receptors including CX3CR1 and CCR2 [32]. On the other hand, Liver infiltrating macrophages, MoMFs, originated from hematopoietic stem cells and is based on hematopoiesis. They can be identified by high CX3CR1, CCR2, Ly-6c, CD11b surface expression [32]. Short-lived circulating Ly-6c^{hi} monocytes are recruited to tissues in homeostasis and injury-associated inflammation [32]. In addition, recruitment of CCR2^{hi} monocytes may promote proinflammatory monocyte accumulation in the liver that has been shown to lead to the development of fibrosis [35].

Because of the heterogeneous features of macrophages, it is difficult to distinguish their subpopulations, especially under inflammatory conditions [32]. Studies in human and murine

models of acute and chronic liver injury have been attempted to discriminate between KCs and MoMFs [36], [37], [38], [39], [40]. However, the recent progress in multiparameter flow cytometry analysis allowed more accurate distinguishing between macrophage subsets [24] [41], [42], [43]. We also used flow cytometry analysis to differentiate subtypes of macrophages and T lymphocytes, and additionally performed immunohistochemistry (IHC).

Immune microenvironment is an important feature in hepatocarcinogenesis [44], [22], [45], therefore, we showed how to analyze hepatic immune cell composition in the early stage of NASH, which can progress to HCC, via flow cytometry and IHC. In this study, we presented how to generate a NASH and explored the changes in hepatic immune microenvironment according to the progression of NASH.

. MATERIALS AND METHODS

1. Experimental animals and housing

All studies were carried out using male C57BL/6N (n=23 mice). Mice were housed in a specific pathogen-free facility, and in a climate controlled room with a temperature of 22±2 , humidity 55±5%, and a 12 hours dark-light cycle. This study was conducted in accordance with regulation of Institutional Animal Care and Use Committee of Asan Medical Center (Permit Number: 2020-02-234).

2. Murine model of Non-alcoholic steatohepatitis

Pathogen-free pregnant C57BL/6N mice (JA BIO) at 14 days of age were purchased, and male pups were used in this study. Two groups: the STAM group and normal group. STAM mice were induced by a single subcutaneous injection of 200 μg of Streptozocin (Sigma-Aldrich, S0130) 2 days after birth followed by feeding with a 60 kcal% fat diet (Research Diets, D12492) after 4 weeks of age. Mice in the normal group were fed a standard diet (Purina).

3. Blood collection and Serum biochemistry

Necropsy was performed at 5, 6, 7 weeks of age. All animals were anesthetized with Terrel Isoflurane to collect blood from inferior vena cava under fasting conditions for 12 hours and sacrificed by exsanguination. Whole blood was collected into serum-separating tubes (BD Microtainer^{R}, 365967) and mixed thoroughly. The blood was centrifuged at 3,000 rpm for 10 minutes to isolate serum and they were used for clinical serum biochemistry analysis.

In this study, serum biomarkers, alanine aminotransferase (ALT), aspartate aminotransferase (AST), triglycerides (TG), glucose, levels were measured using an automated clinical chemistry analyzer (Hitachi, 7180 Clinical Analyzer).

4. Tissue sampling for Flow cytometry analysis and Histopathological evaluation

The livers were sampled for FACS analysis and histopathological evaluation. For the flow cytometry analysis, the half of the left lateral lobe and other remaining lobes except for the median lobe were immediately placed in cold MACS Tissue Storage Solution (Miltenyi Biotec Inc, Auburn CA, USA, 130-100-008) and process for single cell preparation was performed.

For histopathological examinations, both median and the rest of the left lateral lobe were immediately fixed with 10% neutral buffered formalin (MDPOS, 50-00-0) for 24-48 hours then dehydrated in graded ethanol, cleared in xylene using Shandon Excelsior ES tissue processor (Thermo Fisher Scientific), and embedded in paraffin blocks using an EG1150H paraffin-embedding station (Leica Biosystems, Wetzlar, Germany). The paraffin blocks were sectioned in 3 μm thick and uncoated slides (MUTO, 5116-20F) were used for H&E staining, silane coated slides (MUTO, 5116-20F-C) were used for Sirius red and other immunohistochemical staining. The sections were baked in 65 dry-oven for 30-60 minutes and stained with hematoxylin and eosin (Leica, ST5010 Autostainer XL Slide Stainer) and Sirius red (manual protocol) and Immunohistochemical methods (Benchmark XT; Ventana Medical Systems Inc., Tucson, AZ).

5. Single cell preparation for Flow cytometry analysis from liver tissues

Flow cytometry was employed for the characterization of macrophage and T cell subsets in the liver between normal and disease progression. For analysis, liver tissues, left lateral lobe and other remaining lobes except for median lobe were collected at 5, 6, and 7 weeks from

STAM mice. Fresh liver tissue was placed in cold MACS Tissue Storage Solution and rinsed by DMEM/high glucose with L-glutamine, sodium pyruvate (HyClone™, SH30243).

To digest livers, the digestion media composed of DMEM and Enzyme D, R, A which included in MACS Liver Dissociation Kit (Miltenyi Biotec Inc, Auburn CA, USA, 130-105-807) was prepared. Prepared livers were chopped with a surgical scissor in gentleMACS C Tubes (Miltenyi Biotec Inc, Auburn CA, USA, 130-096-334) containing the digestion media (4.7 mL DMEM with 200 µL Enzyme D solution, 100 µL Enzyme R solution, and 20 µL Enzyme A solution per liver). Chopped livers were immediately homogenized using gentle MACS Dissociator with Heaters (Miltenyi Biotec Inc, Auburn CA, USA, 130-096-427) for 35 minutes and which program was 37C_m_LIDK_1. After termination of the program, tissue homogenate was filtered through 100 µm cell strainer (Falcon, 352360) to remove tissue chunks and achieve a single cell suspension and then centrifuged at 2,000 rpm for 3 minutes. Following centrifugation, the supernatants were removed and resuspended with cold-FACS buffer (PBS containing 5% FBS and 2mM EDTA) for washing. Cell suspension was washed twice as mentioned above. To remove RBCs, the digested cells were incubated with 1X RBC Lysis Buffer (1 mL/tissue, eBioScience™, 00-4333-57) for 5 minutes at room temperature and washed with cold-FACS buffer. Single cell suspension was passed through 100 µm cell strainer and counted. After cell counting, the cell suspension was adjusted to $1x10^6$/50 µL cell concentration using FACS buffer for flow cytometry analysis.

6. Flow cytometry analysis of single cells and antibodies

Prepared single cells ($1x10^6$/50 µL) as described above were Fc-blocked using CD16/CD32 antibodies (Abs) (2.4G2, BD Pharmingen™) for inhibiting non-specific binding in FACS buffer for 5 minutes on ICE, and then cells were incubated with flow cytometry antibodies (1:100 dilution) as listed in **Table 1** for 30 minutes at dark on ice. After staining, 150 µL FACS

buffer was added into each sample and centrifuged at 2,000 rpm for 3 minutes for washing. Post first washing step each sample was resuspended with 200 µL FACS buffer and centrifuged as described above. Final washing step was conducted as described above. After centrifugation of final washing, cells were resuspended with 200 µL FACS buffer and all stained samples were assessed using the CytoFLEX Flow Cytometer (Beckman Coulter) and further analyzed using FlowJo software (Tree Star, Ashland, OR, USA).

7. NAFLD Activity Score (NAS) and fibrosis score for disease severity

Histopathologic lesions of NAFLD evaluation were analyzed semi-quantitatively according to the NASH CRN Pathology Committee system for NAS and fibrosis score [46]. The NAS includes evaluation of steatosis, hepatocellular ballooning degeneration, lobular inflammation. To evaluate the severity of the disease, H&E and Sirius red staining were performed to score NAFLD activity and fibrosis, respectively.

8. Immunohistochemical assessment

For identifying hepatic markers, immunohistochemical staining of the liver sections was performed using an automated slide preparation system (Benchmark XT; Ventana Medical Systems Inc., Tucson, AZ). Deparaffinization, epitope retrieval, and immunostaining were performed according to the manufacturer's instructions with EZ Prep Concentration, Cell Conditioning Solutions and the BMK UltraView Universal DAB Detection Kit (#760-500).

Deparaffinization of the liver sections was conducted by EZ Prep (#950-102), a mild detergent solution, with heating. Epitope retrieval was performed by tris based buffer, Cell Conditioning Solution (CC1), with a slightly basic pH. Next, the liver sections were stained with primary antibodies as listed in **Table 2** for 36 minutes at 37 . UltraMap Anti-rabbit HRP

(#760-4315) was used as a secondary antibody for 12 or 16 minutes at 37 . Positive signals were amplified using UltraView DAB and UltraView Copper included UltraView Universal DAB Detection Kit and sections were counterstained with Hematoxylin (#760-2021) and Bluing reagents (#760-2037). The number of CD68, CD163 and CCR2 immunoreactive cells in the liver were quantified in 600 x 400 μm^2 fields using ImageJ software. The positive staining of CD86 in the livers was analyzed qualitatively by comparing staining density [47].

9. Statistical Analysis

All data are presented as mean ± standard deviation (SD). Comparisons between multiple groups were performed with the ANOVA and linear modeling methods $P < 0.05$ was considered statistically significant. Statistical analyses were performed using R.

. RESULTS

Evaluation of liver injury in early stage of steatohepatitis by histological features and serological parameters.

As described in introduction part, NAFLD includes simple steatosis, steatohepatitis that can progress to cirrhosis and HCC. Since the STAM mice have a higher mortality rate as the induction period is longer [29], we decided to study the basis for the occurrence of HCC by focusing on the early stage of NASH. Accordingly, we examined the development of steatosis and the progression to NASH by assessing liver injury at 5, 6 and 7 weeks of STAM mice **(Figure 1)**.

We confirmed that the body weight of the STAM mice was lower than that of the normal mice **(Figure 2, Table 3)** but the liver weight increased as the induction period increased **(Figure 3, Table 4)**. Additionally, mice livers showed remarkable ballooning degeneration of hepatocytes and mild steatosis. Overall, lobular inflammation was identified in 1-2 foci in x200 high power field (HPF). The degree of liver injury was most severe at 7 weeks. Fibrosis was minimally observed on portal tracts or sinusoids in Sirius red staining. But, no remarkable differences between groups. We scored liver tissue sections using NAFLD activity score (NAS) to evaluate the histopathology of NASH **(Figure 5, Table 6)**.

In two mice in the 7 weeks group, well defined nodule was identified in each mouse. Both nodules showed small cell changes, minimal to mild nuclear atypia and absence of portal tracts. Solitary artery was not identified. Cell density was counted manually in central portions of nodules and adjacent parenchyme of both lesions. It was found that the cell density of nodules was more than twice that of the surrounding livers. From these results, it was presumed that

these lesions were early hepatocellular carcinomas. Confirmative studies such as reticulin and CD34 staining were not performed.

Next, we measured the serological parameters such as AST, ALT, TG, glucose. The AST, ALT levels were elevated at all periods compared to normal mice. TG levels seemed to decrease at 5 weeks compared to normal mice, but gradually increased minimally. Glucose levels were increased in all periods compared to normal mice, and showed a significantly higher level, especially at 6 and 7 weeks **(Figure 4, Table 5)**.

STAM mice results in emergence of infiltrating macrophages.

To determine how the STAM model affects resident and circulating macrophage recruitment, we analyzed macrophage subpopulations **(see Figure 6 for gating strategy)** using flow cytometry. The percentage of pan-macrophages labeled with $F4/80^{hi}$ in the liver showed an increasing pattern from the 6 weeks. In addition, the proportion of monocyte-derived infiltrating macrophages labeled with $CD11b^{hi}$ $Ly\text{-}6c^{hi}$ within $F4/80^{hi}$ cells were increased from the 5 weeks. On the other hand, no notable changes were observed in liver resident macrophages labeled with $CD11b^{low}$ $Ly\text{-}6c^{low}$ cells **(Figure 8)**.

As described above, we explored subgroups of hepatic macrophages using flow cytometry, but we wanted to obtain conclusive results through further experiments. Accordingly, we attempted to differentiate between KCs and MoMFs by performing immunohistochemical staining. We used CD68 as a marker of pan-macrophages and CCR2 as a marker of MoMFs. Meanwhile, in the case of KCs, it was indirectly predicted by comparing the ratio of $CCR2^{+}$ cells to $CD68^{+}$ cells. To investigate the macrophage subpopulations, we counted the number of $CD68^{+}$, $CCR2^{+}$ cells **(Figure 9, Table 7, 8)**. Compared with normal mice, the number of $CD68^{+}$ cells in STAM groups showed an increase, but no difference was observed between induction periods. On the other hand, the number of $CCR2^{+}$ cells indicate a gradual increase as the induction period increased **(Figure 8)**.

STAM mice showed a reduction of M2 macrophages.

As mentioned above, we confirmed that as the NAFLD progressed, the activity of MoMFs circulating through the blood became more prominent. Another approach was attempted from the perspective of M1 and M2 macrophages. Immunohistochemical staining was performed with CD163 as a marker for M2 macrophage. We observed that the number of $CD163^{+}$ cells was decreased throughout disease **(Figure 10, Table 9)**. In other words, the proportion of M2 macrophages in the liver decreased as the disease progressed.

Confirmative studies to identify M1 macrophages such as peroxisome proliferator-activated receptor (PPAR), CCL2, CD80, and CD86 staining were not performed. It was difficult to confirm that the activity of M1 macrophages was prominent as the NASH progressed, but we could speculate that the M1/M2 balance was disrupted.

$CD8^+$ T cells may play a critical role in STAM NASH.

As previously described, we considered macrophages to play a key role in NASH, but further investigated T cells contributing to the evolution of hepatic inflammation **(see Figure 7 for gating strategy)**. Since we focused on the early stages of NASH, it was difficult to observe a massive inflammation, but we could find a certain tendency of $CD8^+$ T cells. This trend was confirmed by flow cytometry and immunohistochemical staining and, as NASH progressed, the number of infiltrating $CD8^+$ T cells in the liver increased **(Figure 11, 12, Table 11)**. However, it was difficult to observe this trend in $CD4^+$ T cells in the liver **(Figure 11, 12, Table 10)**.

. DISCUSSION

With an increased incidence of NASH and NASH-to-HCC transition, it is important to predict the pathophysiology of the disease using human-like animal models. In this study, we tried to analyze the hepatic immune microenvironment in early stage of NASH using STAM model. Compared with previous studies that induced NASH through only diet, the STAM mice treated with a toxic substance to pancreatic beta cells and fed a high fat diet would metabolically reproduce to that of humans. In this study of STAM model, we observed the following key findings. In macrophages, it was found that as NASH progressed, the activity of MoMFs was gradually increased than that of KCs. Additionally, the number of M2 macrophages was decreased throughout the disease state when compared to the normal state. In lymphocytes, as NASH progressed, the activity of $CD8^+$ T cells became more prominent than that of $CD4^+$ T cells.

In this study, we analyzed the STAM model, which is thought to be most similar to the human liver microenvironment, using two methods such as flow cytometry and IHC. To the best of our knowledge, this is the first trial to study immune microenvironment using the two previously mentioned techniques in the STAM model. This study provides the value of studying the hepatic immune microenvironment in the STAM model from early to late stages in more detail using diverse markers.

In flow cytometry analysis, we noted an increased influx of blood monocytes labeled with Ly-$6c^{hi}$ $CD11b^{hi}$ gated on $F4/80^{hi}$ during NASH development. Comparison of the normal and disease-induced groups revealed their roles in triggering NASH by allowing the recruitment of blood monocytes. We also confirmed the distribution of T cell subgroups, and observed an increase in $CD8^+$ T cells as NASH progressed.

In the case of immunohistochemical staining, these analyses were not executed using the same markers used in flow cytometry, but similar trend could be identified by labeling alternative markers. The activity of monocyte-derived infiltrating macrophages labeled with CCR2 became more prominent as the NASH progressed. It was also identified that the pan-macrophages labeled with CD68 increased throughout the disease state. Based on these tendencies in flow cytometry and immunohistochemistry staining results, we attempted to approach them from the perspective of M1 and M2 macrophages to better understand the hepatic microenvironment. The number of M2 macrophages labeled with CD163 decreased throughout the NASH development, and from this result, we could indirectly infer that the activity of M1 macrophages was increased. Therefore, we speculated that the inflammatory microenvironment originated from the beginning of the onset of NAFLD will influence any disease that may develop thereafter.

As mentioned above, we confirmed that $CD8^+$ T cells and $CCR2^+$ macrophages increased in number along with NASH progression. When compared to human NASH, elevation in CD8 staining positively correlated with α-smooth muscle actin (α-SMA) [48]. Increased $CCR2^+$ macrophages parallel to NASH severity and fibrosis stage in another immunohistochemical results of humans as well [49]. Referring to the results of these previous studies, we identified that there was a similarity between the humans and STAM mice.

However, this present study has the following limitations. First, the interpretation is limited by the small number of mice in the NASH subgroups (n=6, n=5, and n=6, respectively) and therefore requires further validation. In addition, although the STAM model has the advantage of showing most of the NAFLD spectrum, it was difficult to investigate up to the end-stage because sufficient number of animals were not secured. The second limitation was the fact that relatively basic parameters were used. If we had explored additional markers, such as cytokines, associated with the inflammatory microenvironments, the results would have given

us more information. Third, the markers of the two methods, flow cytometry and IHC, used in this study were not identical. Although similar patterns were observed in both methods, it would have shown more confirmative data if they were carried out with same markers.

In conclusion, this present study provides evidences that $CD8^+$ T cells and $CCR2^+$ macrophages are increased in number along with NASH progression. Although it is necessary to investigate in more detail through additional studies with additional markers in a sufficient number of animals, these results are the first attempt to study the hepatic immune microenvironment using flow cytometry and IHC in a STAM model.

FIGURES AND TABLES

Figure 1

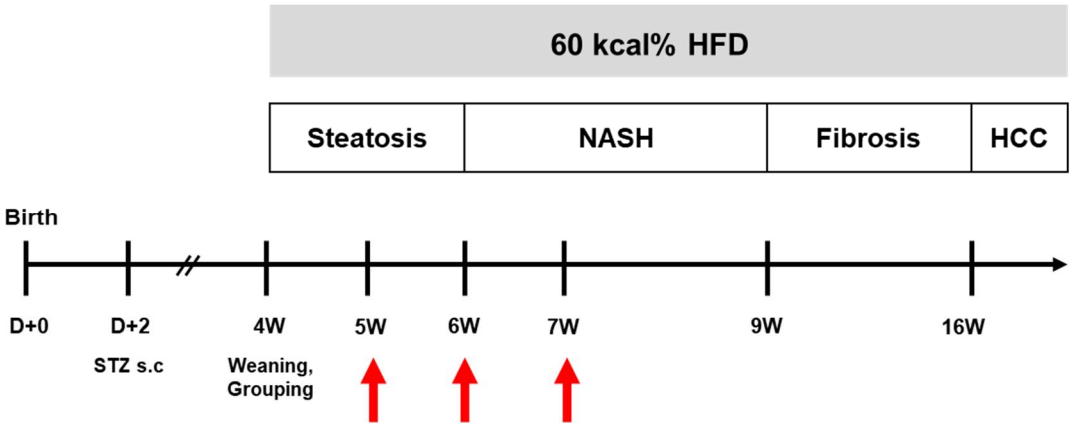

Figure 1. Timeline of the development of steatosis, NASH, Fibrosis, and HCC in STAM mice. The schematic represents timeline of data collection (red arrows) during induction period (n=5-6/group). HCC, hepatocellular carcinoma; HFD, high fat diet; NASH, non-alcoholic steatohepatitis; STZ, streptozocin.

Figure 2

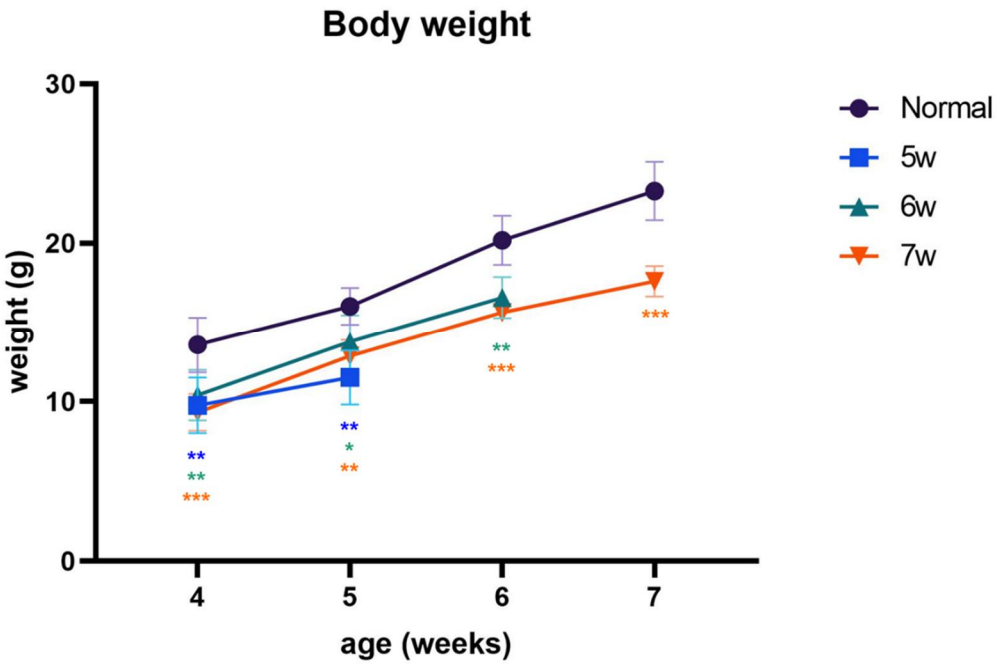

Figure 2. Changes in body weight according to the ages in STAM mice. The STAM mice weighed less than the normal mice, but increased in proportion to the induction period. Data are expressed as mean ± standard deviation (SD) of n=5-6 mice per group. * $p < 0.05$ versus normal group, ** $p < 0.01$ versus normal group, *** $p < 0.001$ versus normal group.

Figure 3

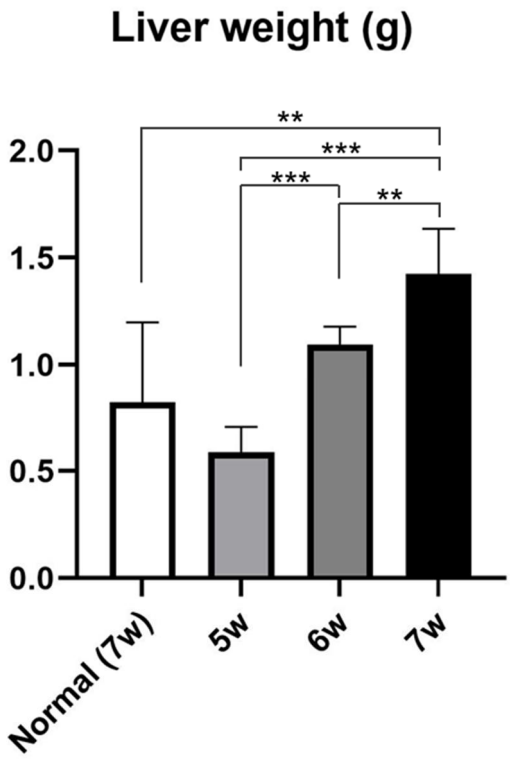

Figure 3. Changes in liver weight according to induction period in STAM mice. The weight of livers from STAM mice increased proportionally with the induction period. Data are expressed as mean ± standard deviation (SD) of n=5-6 mice per group. ** $p < 0.01$, *** $p < 0.001$.

Figure 4

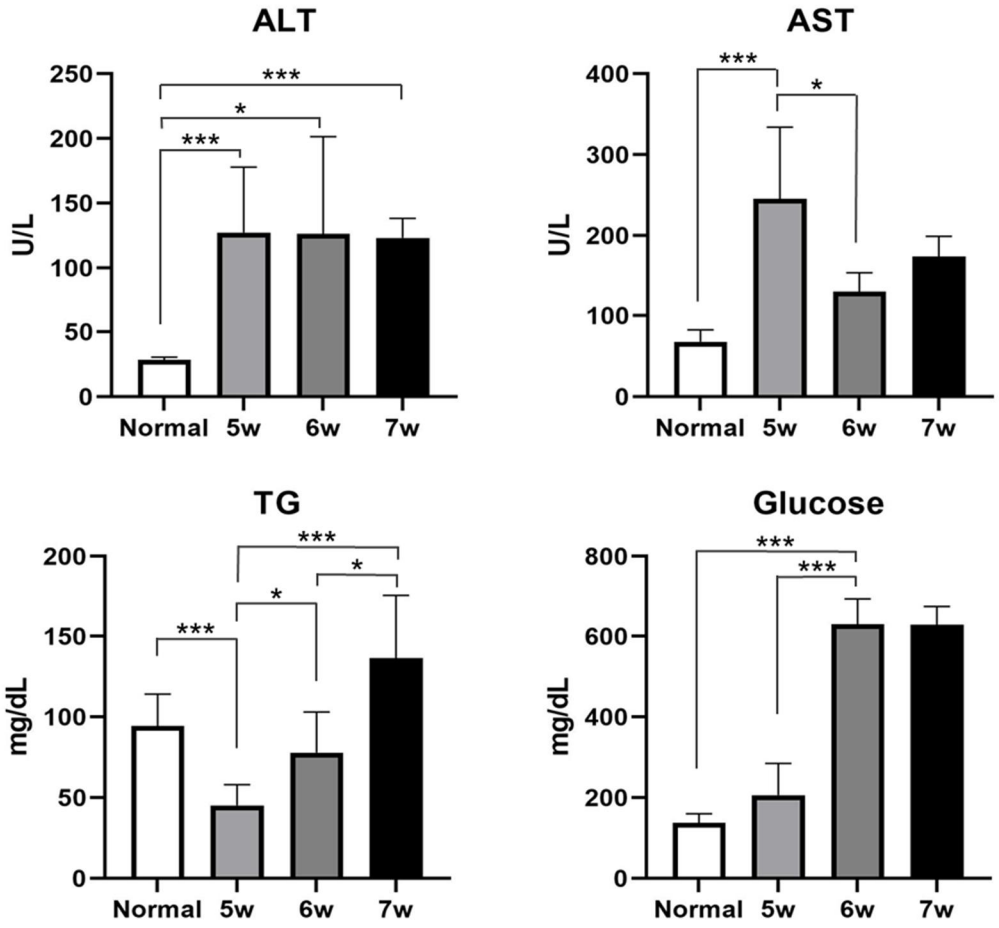

Figure 4. Result of serum chemistry values. ALT, AST levels are significantly elevated after 5 weeks of STAM mice compared to Normal mice. TG level seemed to decrease compared to normal mice at the beginning of induction, but gradually increased. Glucose level was increased in all periods compared to the normal mice, and it was particularly high at 6 and 7 weeks. Data are expressed as mean ± standard deviation (SD) of n=5-6 mice per group. * $p < 0.05$, *** $p < 0.001$.

Figure 5

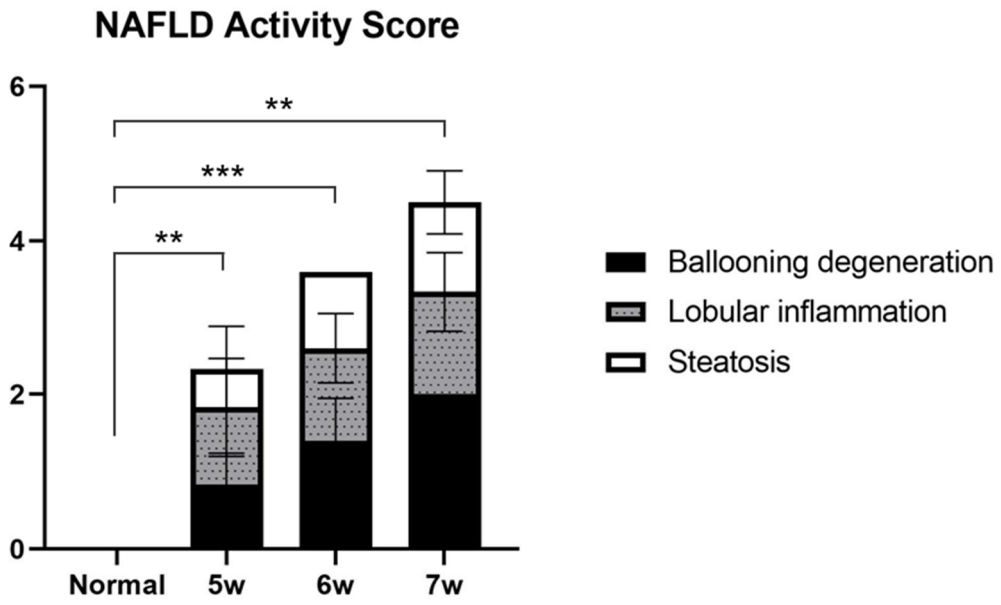

Figure 5. Result of NAFLD Activity Score. The longer the induction period, the higher the score. Data are expressed as mean ± standard deviation (SD) of n=5-6 mice per group. ** $p < 0.01$, *** $p < 0.001$.

Figure 6

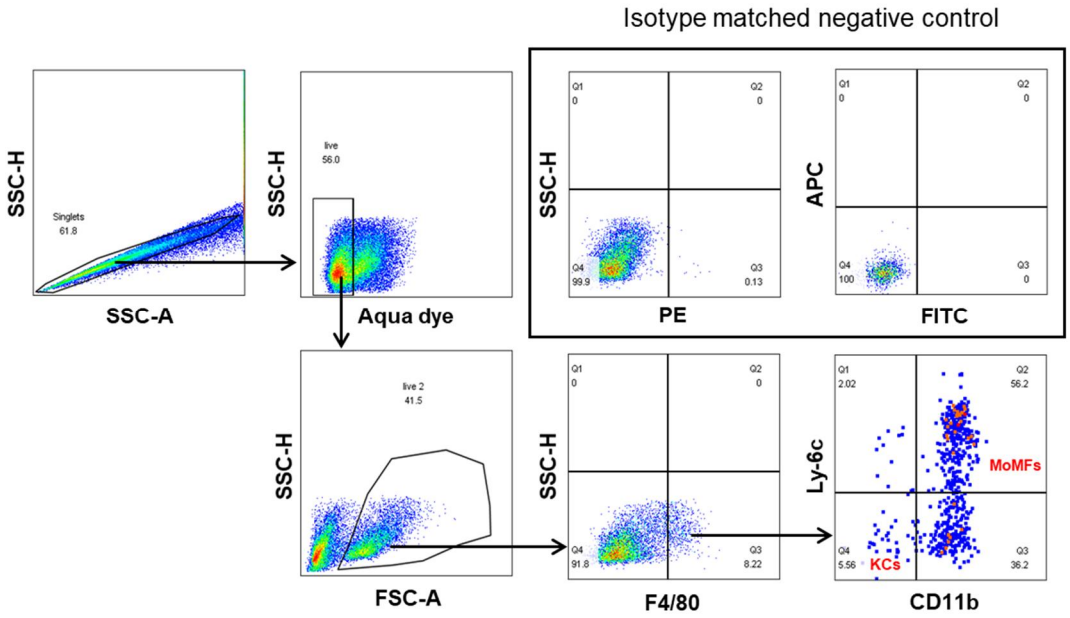

Figure 6. Gating strategy used to identify hepatic macrophages population. MoMFs, KCs from STAM and normal mouse liver tissues. Liver-derived single cells were stained with fluorophore-labeled anti-F4/80, CD11b, Ly-6c together with Aqua fluorescent reactive dye (dead cell staining). FSC, forward scatter; SSC, side scatter.

Figure 7

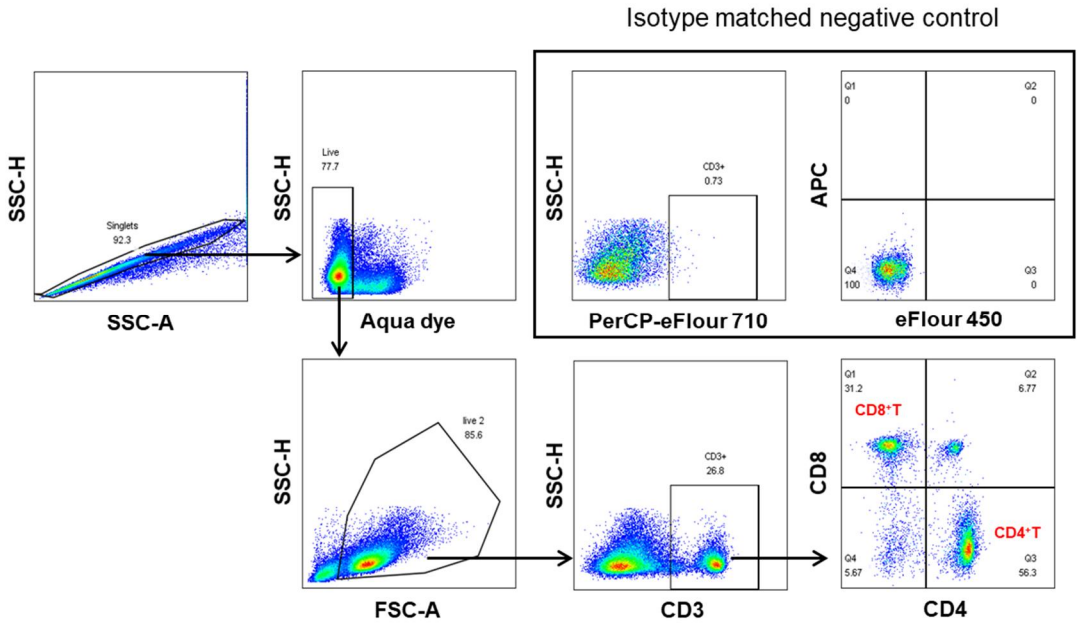

Figure 7. Gating strategy used to identify liver infiltrated T lymphocytes population. $CD4^+$ T cells, $CD8^+$ T cells from STAM and normal mouse liver tissues. Liver-derived single cells were stained with fluorophore-labeled anti-CD3, CD4, CD8 together with Aqua fluorescent reactive dye (dead cell staining). FSC, forward scatter; SSC, side scatter.

Figure 8

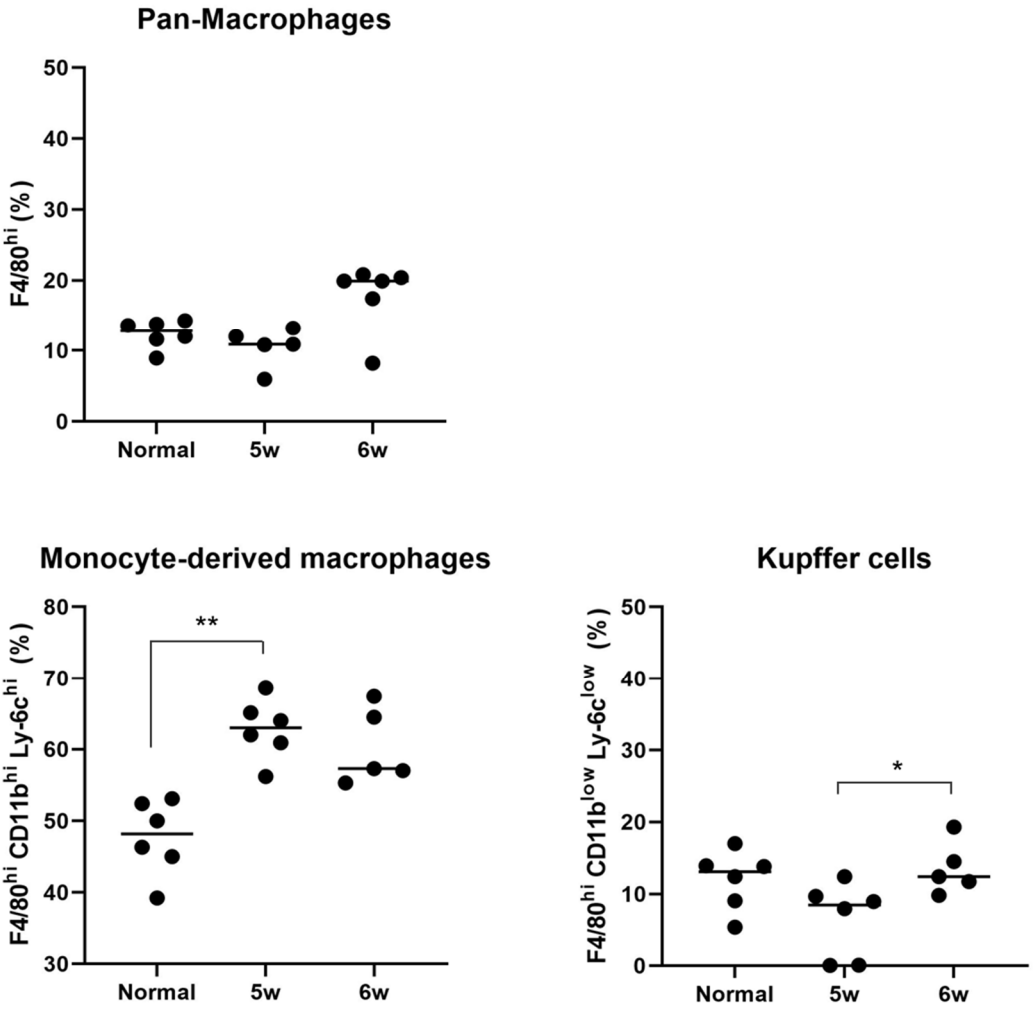

Figure 8. Composition of hepatic macrophages in Flow cytometry. Data represent 5-6 mice per group and the line represents the mean of a data. * $p < 0.05$, ** $p < 0.01$.

Figure 9

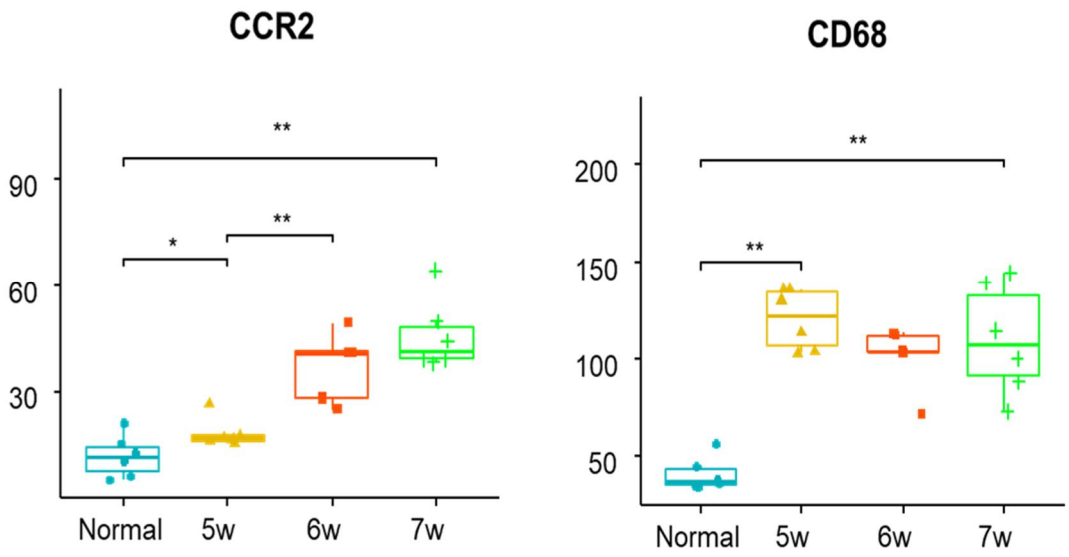

Figure 9. Number of cells stained positive for CCR2 and CD68 in immunohistochemistry. The top of the box represents the 75% of the data, the bottom of the box represents the 25% of the data, and the line in the middle represents the median of a data. The whiskers represent the highest and lowest values that are not outliers. Individuals beyond the whiskers represent outliers and extreme values. * $p < 0.05$, ** $p < 0.01$.

Figure 10

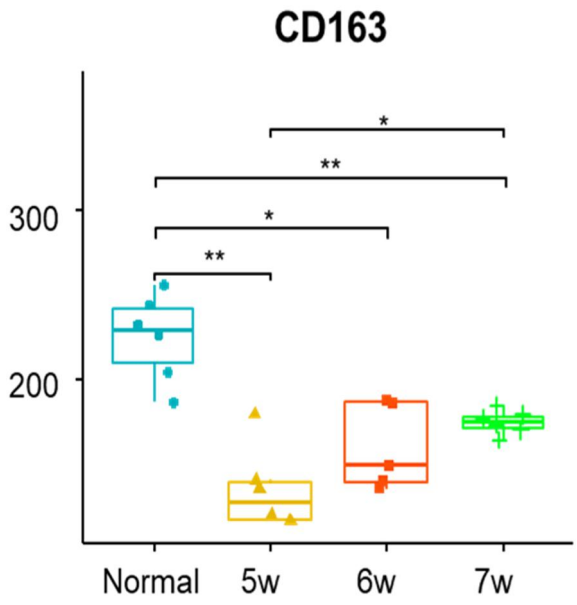

Figure 10. Number of cells stained positive for CD163 in immunohistochemistry. The top of the box represents the 75% of the data, the bottom of the box represents the 25% of the data, and the line in the middle represents the median of a data. The whiskers represent the highest and lowest values that are not outliers. Individuals beyond the whiskers represent outliers and extreme values. * $p < 0.05$, ** $p < 0.01$.

Figure 11

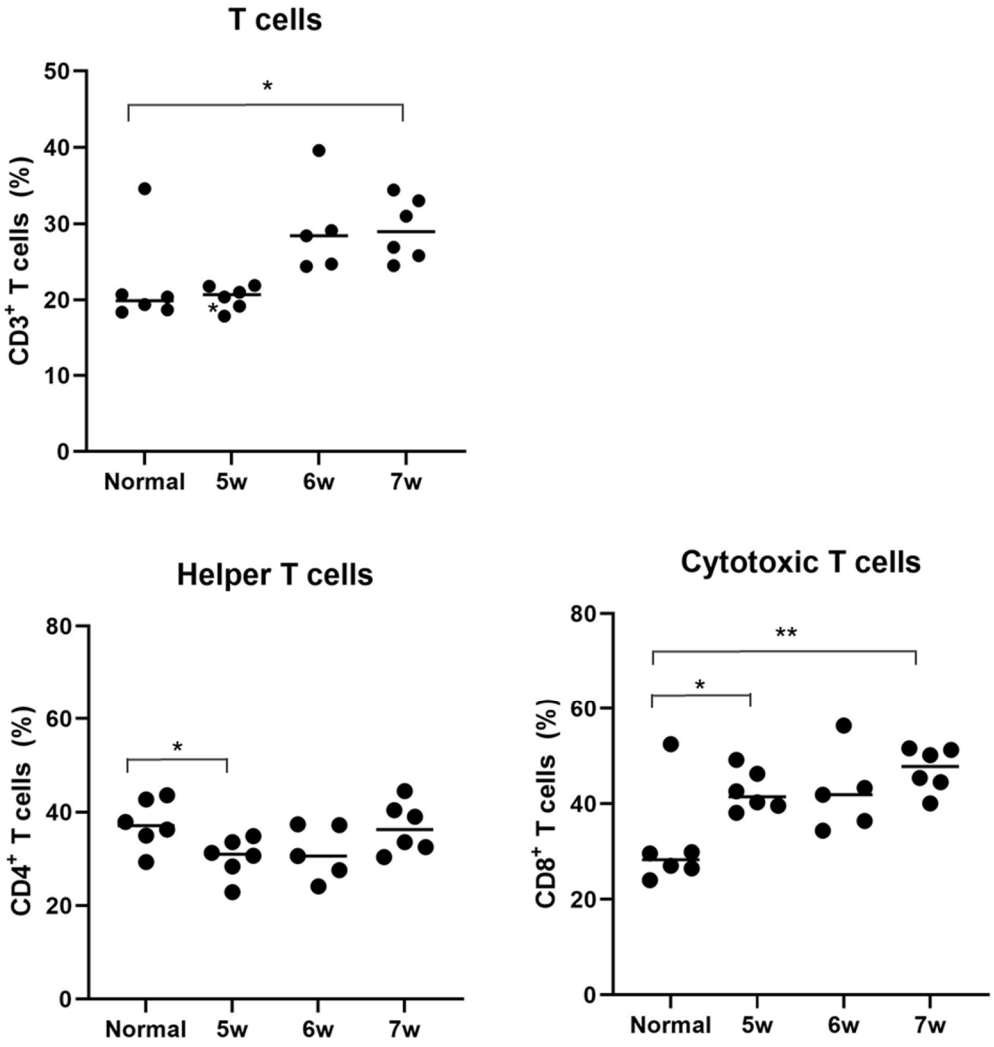

Figure 11. Composition of hepatic T cells in Flow cytometry. Data represent 5-6 mice per group and the line represents the mean of a data. * $p < 0.05$, ** $p < 0.01$.

Figure 12

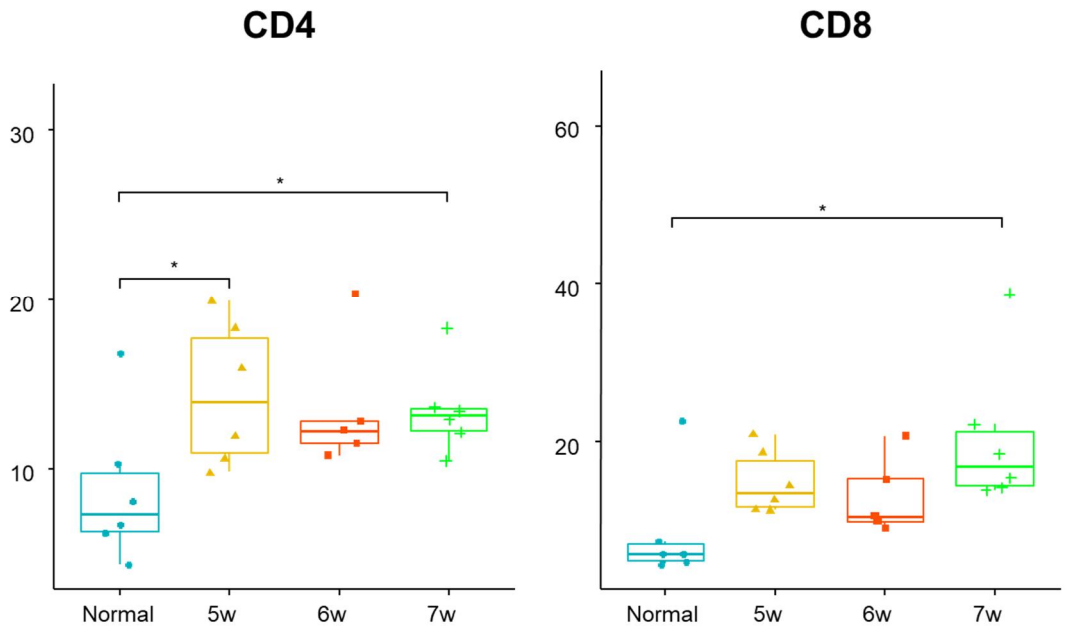

Figure 12. Number of cells stained positive for CD4 and CD8 T cells in immunohistochemistry. The top of the box represents the 75% of the data, the bottom of the box represents the 25% of the data, and the line in the middle represents the median of a data. The whiskers represent the highest and lowest values that are not outliers. Individuals beyond the whiskers represent outliers and extreme values. * $p < 0.05$.

Figure 13

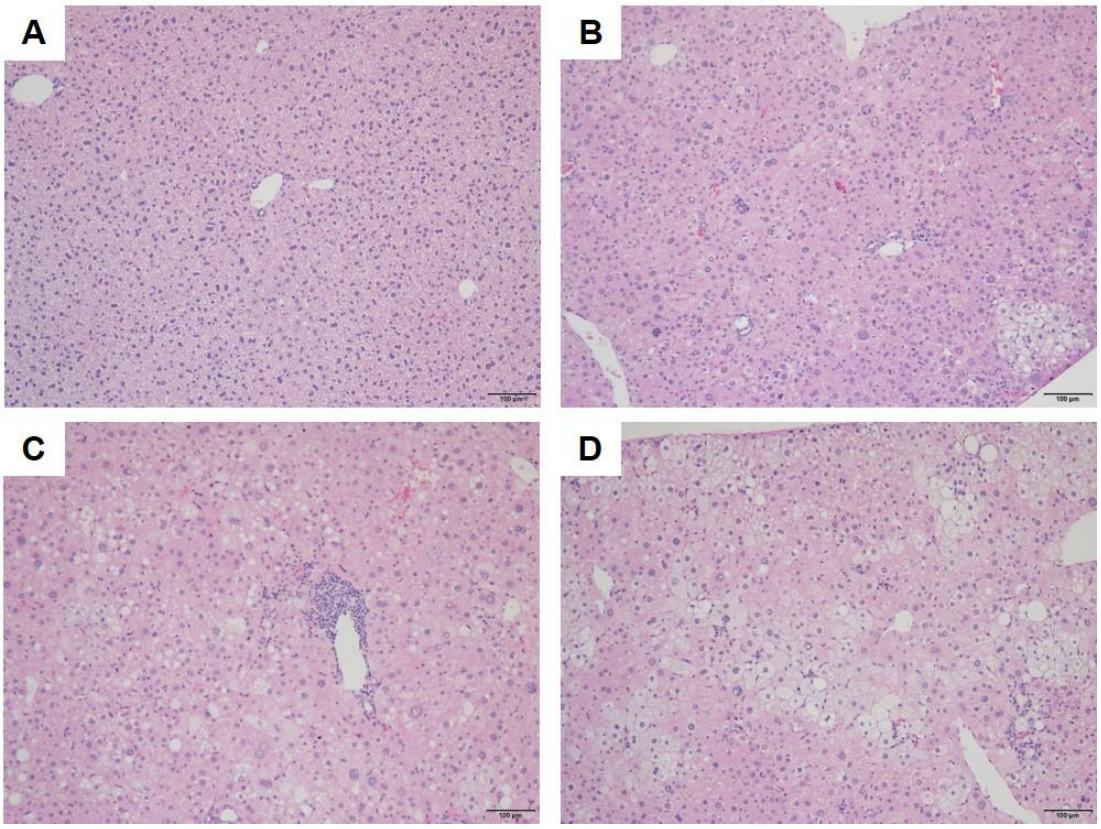

Figure 13. Representative images of H&E stained liver sections (x100). (A) Normal, (B) 5 weeks, (C) 6 weeks, (D) 7 weeks of STAM mice liver.

Figure 14

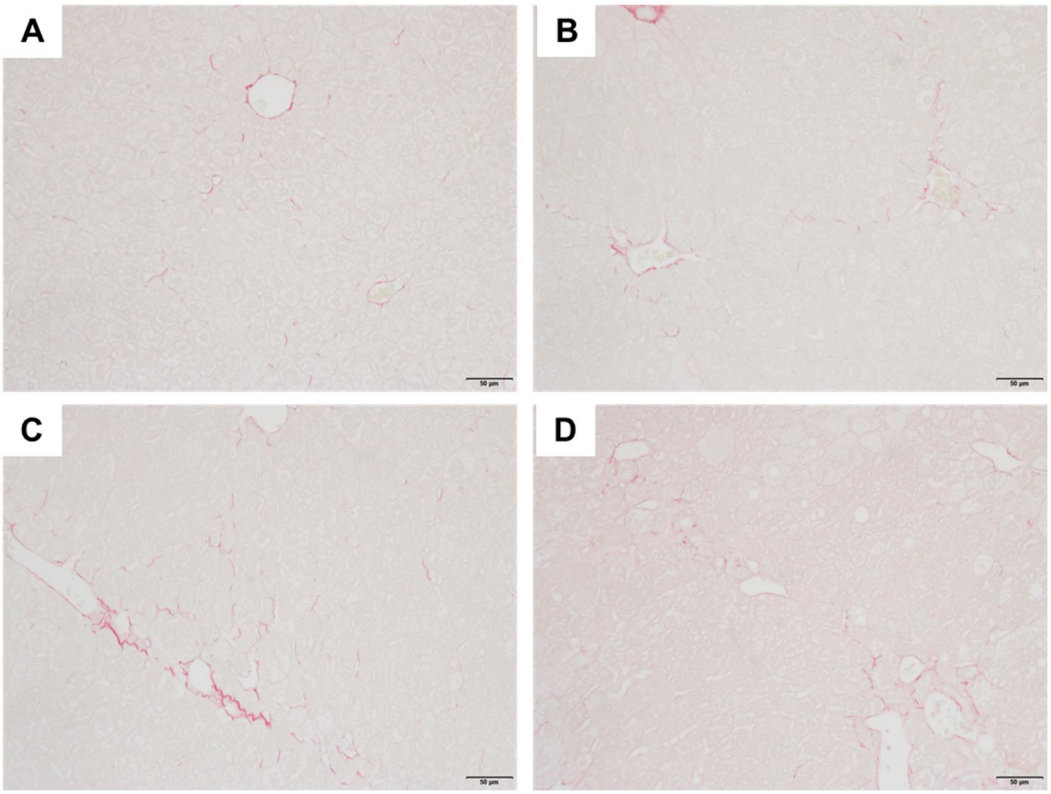

Figure 14. Representative images of Sirius red stained liver sections (x200). (A) Normal, (B) 5 weeks, (C) 6 weeks, (D) 7 weeks of STAM mice liver.

Figure 15

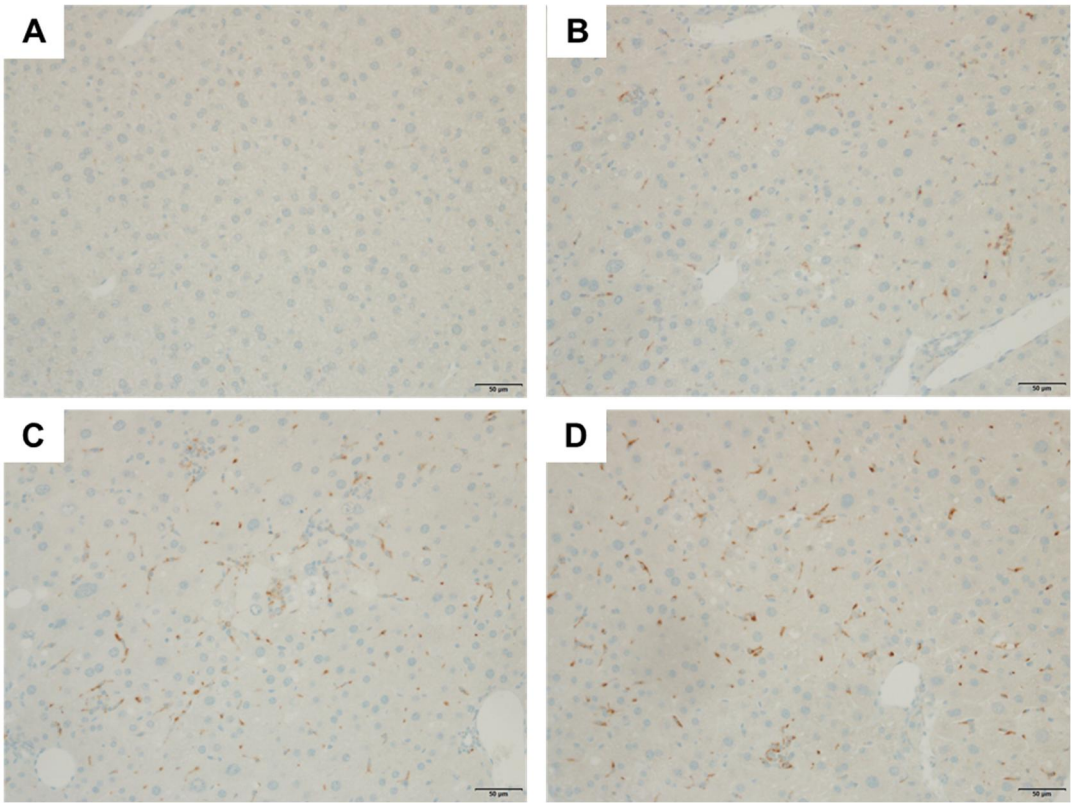

Figure 15. Representative images of CD68^{+} immunohistochemical stained liver sections (x200). (A) Normal, (B) 5 weeks, (C) 6 weeks, (D) 7 weeks of STAM mice liver.

Figure 16

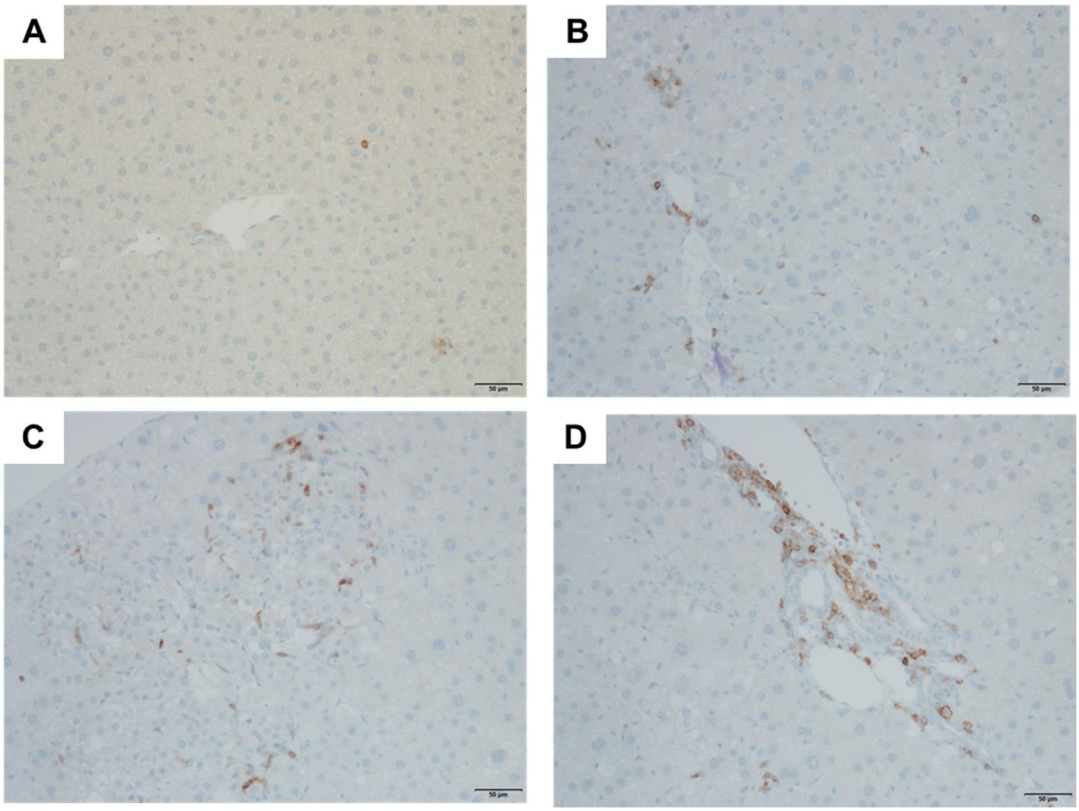

Figure 16. Representative images of CCR2^{+} immunohistochemical stained liver sections (x200). (A) Normal, (B) 5 weeks, (C) 6 weeks, (D) 7 weeks of STAM mice liver.

Figure 17

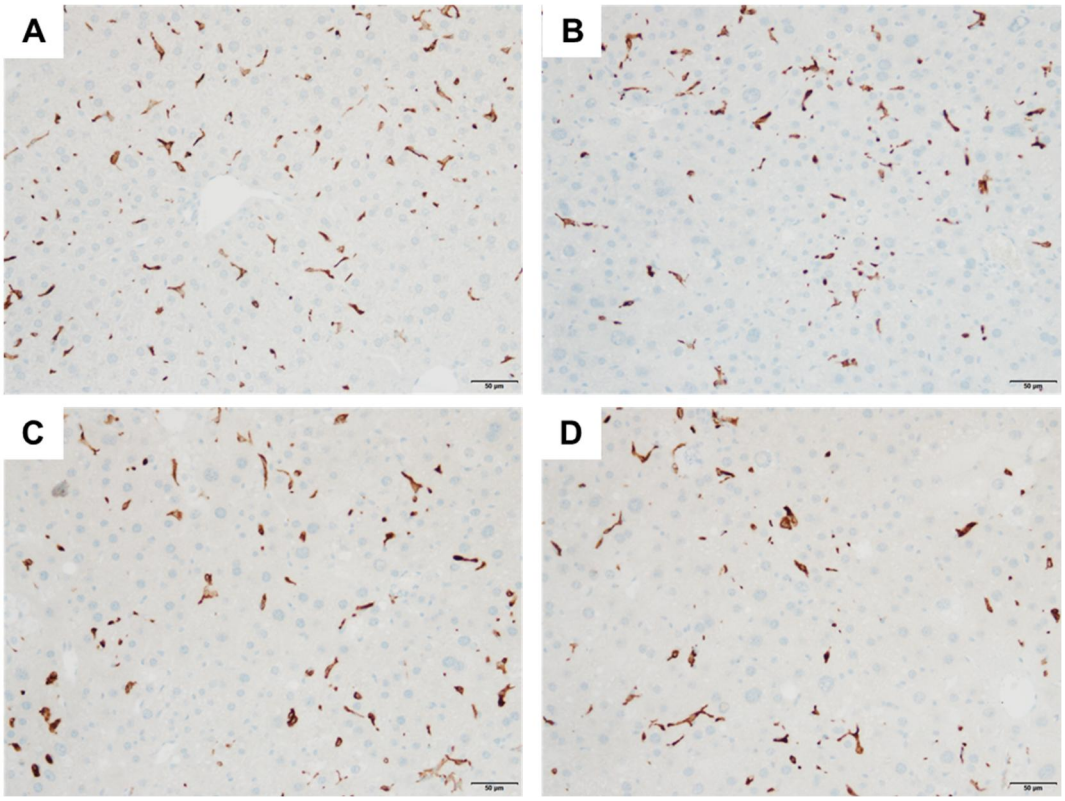

Figure 17. Representative images of CD163^{+} immunohistochemical stained liver sections (x200). (A) Normal, (B) 5 weeks, (C) 6 weeks, (D) 7 weeks of STAM mice liver.

Figure 18

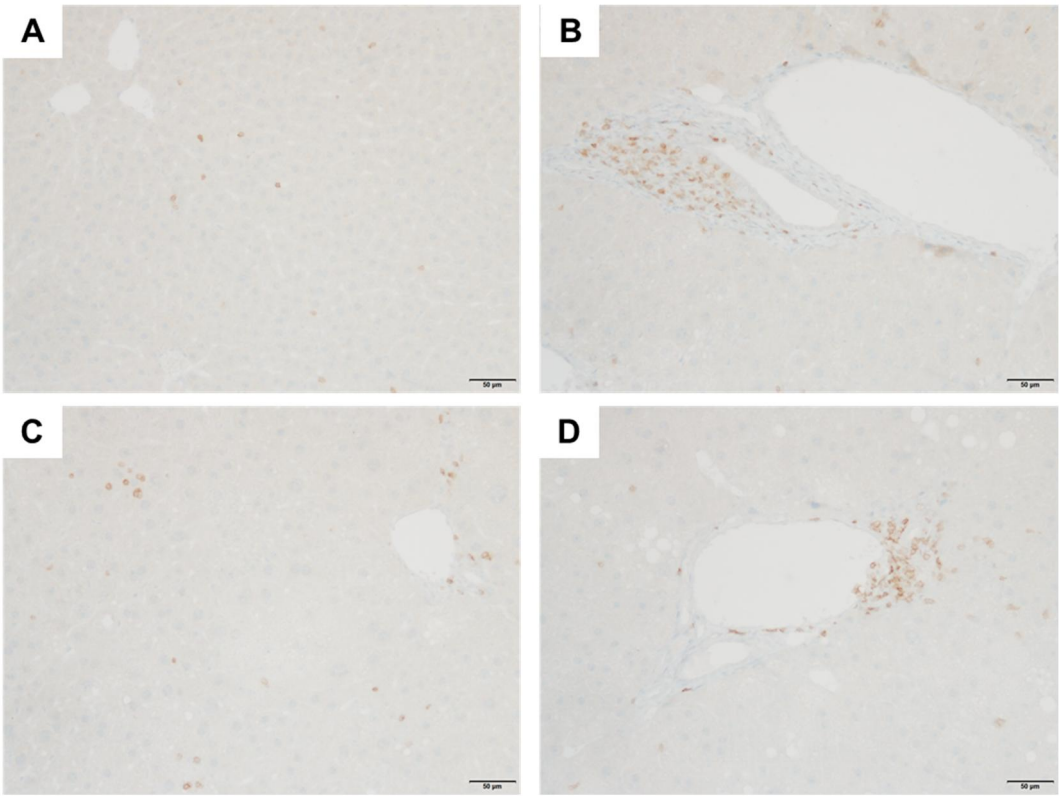

Figure 18. Representative images of CD3$^+$ immunohistochemical stained liver sections (x200). (A) Normal, (B) 5 weeks, (C) 6 weeks, (D) 7 weeks of STAM mice liver.

Figure 19

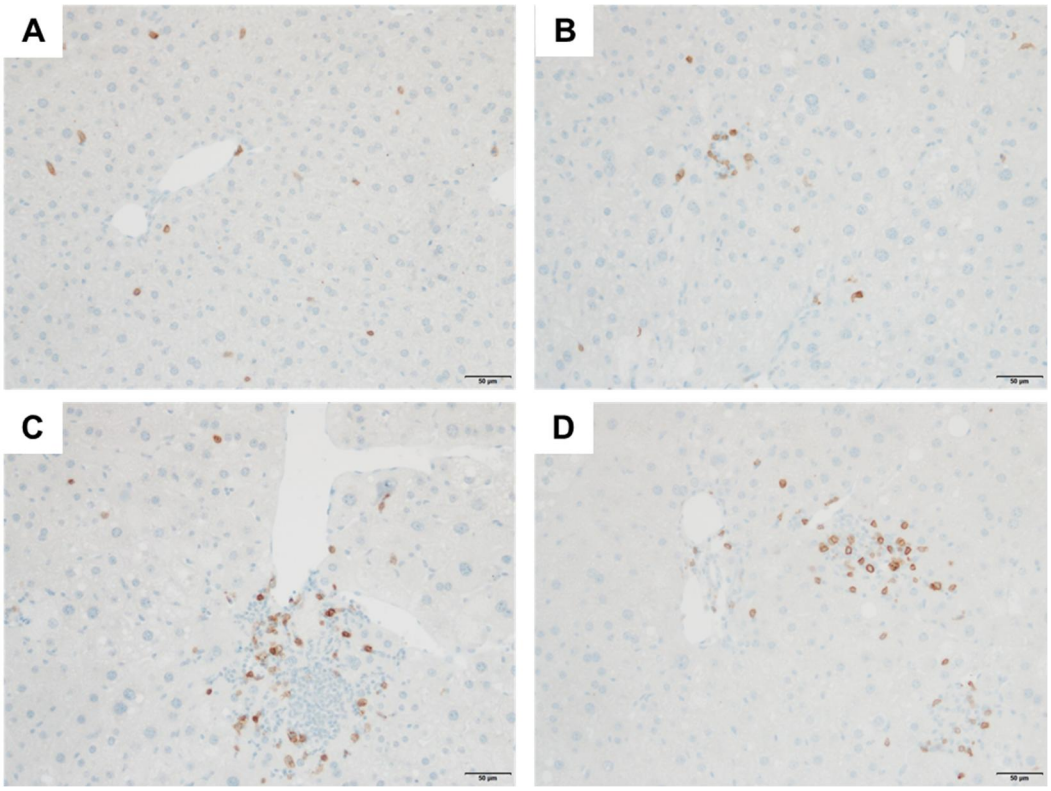

Figure 19. Representative images of CD4$^+$ immunohistochemical stained liver sections (x200). (A) Normal, (B) 5 weeks, (C) 6 weeks, (D) 7 weeks of STAM mice liver.

Figure 20

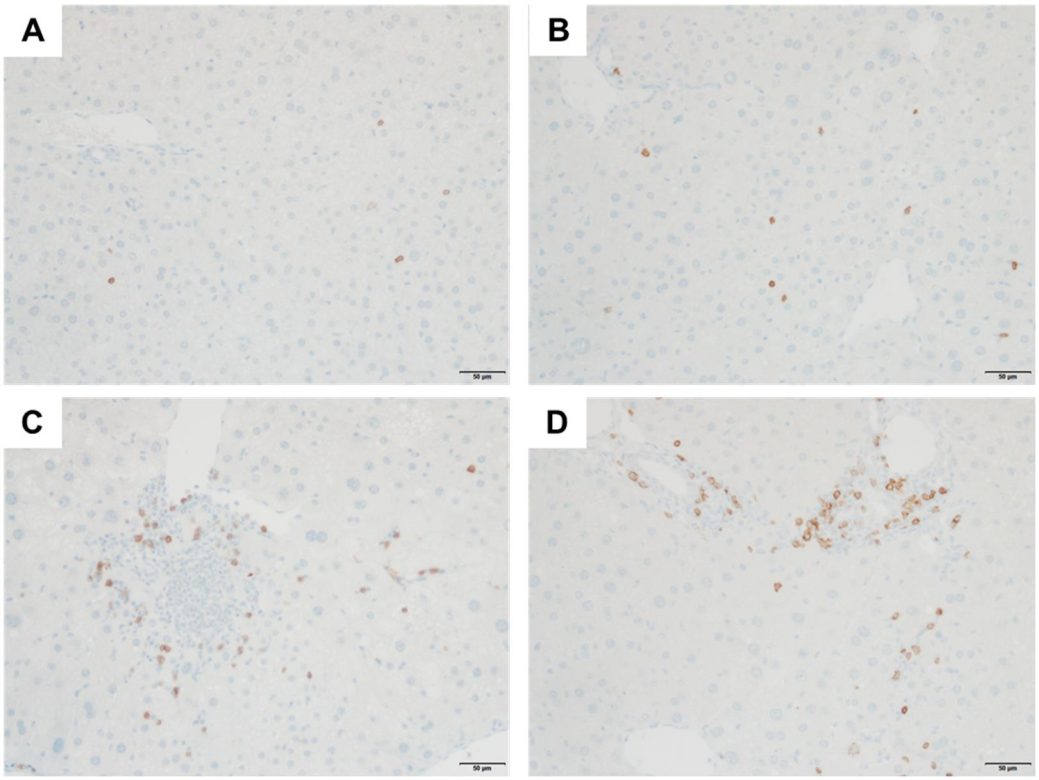

Figure 20. Representative images of CD8$^+$ immunohistochemical stained liver sections (x200). (A) Normal, (B) 5 weeks, (C) 6 weeks, (D) 7 weeks of STAM mice liver.

Table 1

Table 1. The list of antibodies used for Flow cytometry analysis in this study.

#	Antibody	Company	Clone	Cat. #
1	Anti-Mouse F4/80	eBioscience	BM8	41-4801-82
2	Anti-Mouse Ly-6C	BD Pharmingen	AL-21	560595
3	Anti-Mouse CD11b	eBioscience	M1/70	11-0112-41
4	Anti-Mouse CD3	eBioscience	17A2	46-0032-82
5	Anti-Mouse CD4	eBioscience	RM4-5	48-0042-82
6	Anti-Mouse CD8a	eBioscience	53-6.7	17-0081-82
7	Anti-Mouse CD16/32	BD Pharmingen	2.4G2	553142
8	Fixable Aqua Dead Cell Stain Kit	Invitrogen	-	L34957

Table 2

Table 2. Antibody information used for the Immunohistochemical staining in this study.

#	Antibody	Company	Dilution	Primary antibody incubation time (min)	Secondary antibody incubation time (min)	Cat. #
1	Anti-CD3	Abcam	1:400	36	16	ab16669
2	Anti-CD4	Abcam	1:1000	36	16	ab183685
3	Anti-CD8	Abcam	1:2000	36	16	ab217344
4	Anti-CD68	Abcam	1:800	36	12	ab125212
5	Anti-CD86	Invitrogen	1:1000	36	16	PA5-88284
6	Anti-CD163	Abcam	1:1000	36	16	ab182422
7	Anti-CCR2	Abcam	1:500	36	12	ab273050

Table 3

Table 3. Individual body weight values (g).

Group	Animal No.	4 weeks	5 weeks	6 weeks	7 weeks
5 weeks	1	10.43	11.65	-	-
	2	10.04	12.01	-	-
	3	12	13.55	-	-
	4	10.45	12.48	-	-
	5	8.82	10.76	-	-
	6	6.9	8.58	-	-
6 weeks	1	9.04	12.5	15.75	-
	2	11.65	15.02	17.61	-
	3	8.82	11.56	14.94	-
	4	12.41	15.51	18.51	-
	5	10.15	14.22	16.02	-
7 weeks	1	7.27	10.94	15.09	15.92
	2	10.36	13.73	15.37	17.54
	3	8.97	12.85	15.99	17.87
	4	10.45	13.58	15.76	17.7
	5	9.41	13.32	16.21	18.86
	6	9.53	12.82	15.35	17.69
Normal (7 weeks)	1	16.45	18.03	21.98	24.83
	2	13.32	15.05	19.39	21.87
	3	14.26	16.39	20.12	24.8
	4	13.35	16.18	21.28	24.88
	5	12.76	15.71	20.7	22.72
	6	11.26	14.78	17.61	20.59

Table 4

Table 4. Individual liver weight values (g).

Group	Animal No.	weight (g)
5 weeks	1	0.68055
	2	0.62331
	3	0.70225
	4	0.63409
	5	0.46927
	6	0.41269
6 weeks	1	1.14957
	2	1.11670
	3	0.95053
	4	1.11863
	5	1.14746
7 weeks	1	1.39488
	2	1.38893
	3	1.39434
	4	1.38934
	5	1.81580
	6	1.16918
Normal (7 weeks)	1	1.03742
	2	0.08801
	3	1.06816
	4	1.07036
	5	0.88334
	6	0.77931

Table 5

Table 5. Individual serum biochemistry values.

Group	Animal No.	Glucose (mg/dL)	AST (U/L)	ALT (U/L)	TG (mg/dL)
Normal	1	103.90	76.80	26.30	74.30
	2	121.60	92.70	31.30	79.80
	3	157.00	56.10	28.40	110.80
	4	131.80	58.80	30.70	91.90
	5	162.80	54.60	25.70	84.10
	6	149.10	68.10	27.70	125.70
5 weeks	1	297.80	240.20	115.80	28.00
	2	215.10	161.10	99.30	38.70
	3	295.80	205.30	84.10	55.40
	4	176.00	228.50	124.80	48.10
	5	106.90		226.40	37.50
	6	147.70	394.50	114.40	63.40
6 weeks	1	605.60	163.60	128.20	96.40
	2	653.30	130.90	87.20	67.40
	3	644.10	119.00	80.10	82.80
	4	711.90	110.40	80.30	40.10
	5	535.70		256.20	103.10
7 weeks	1	555.20	198.40	116.30	
	2	616.00	187.70	138.40	129.30
	3	601.90	169.50	123.40	83.40
	4	671.70	162.00	126.60	168.00
	5	655.00	195.20	137.30	
	6	675.70	133.00	97.30	165.00

(Blanks were judged to be over limit values and excluded from the results)

Table 6

Table 6. NAS scoring.

Group	Animal No.	Ballooning degeneration	Lobular inflammation	Steatosis
Normal	1	0	0	0
	2	0	0	0
	3	0	0	0
	4	0	0	0
	5	0	0	0
	6	0	0	0
5 weeks	1	1	0	1
	2	1	1	0
	3	1	1	0
	4	1	1	0
	5	0	1	1
	6	1	2	1
6 weeks	1	1	1	1
	2	1	1	1
	3	1	1	1
	4	2	1	1
	5	2	2	1
7 weeks	1	2	2	1
	2	2	1	1
	3	2	2	1
	4	2	1	1
	5	2	1	1
	6	2	1	2

Table 7

Table 7. $CD68^+$ cells scoring in immunohistochemistry.

Group	Animal No.	ROI 1	ROI 2	ROI 3	ROI 4	ROI 5	ROI 6	ROI 7	ROI 8	ROI 9	ROI 10
Normal	1	40	45	49	17	37	36	40	37	47	37
	2	81	53	51	70	34	53	90	44	49	50
	3	38	43	30	32	45	33	30	38	30	47
	4	27	47	43	29	32	29	35	42	34	32
	5	30	28	29	30	50	39	43	30	41	37
	6	39	62	43	47	46	45	29	50	48	42
5 weeks	1	141	84	143	124	154	104	98	98	96	100
	2	97	109	99	122	72	122	99	93	111	119
	3	108	68	71	100	102	123	89	155	104	116
	4	131	114	116	102	193	152	136	146	134	137
	5	122	128	157	150	86	128	145	145	123	121
	6	119	112	139	140	146	135	127	164	168	112
6 weeks	1	69	98	74	74	94	59	47	60	68	73
	2	56	149	89	114	121	100	138	138	109	106
	3	80	141	108	111	103	106	86	98	105	100
	4	104	106	115	99	100	107	97	103	116	95
	5	123	98	84	179	87	92	117	101	156	99
7 weeks	1	143	108	109	112	106	120	105	124	123	97
	2	59	98	96	66	76	51	77	81	60	68
	3	173	148	166	131	125	139	133	172	133	124
	4	109	99	115	88	102	77	81	93	117	123
	5	100	113	186	160	124	215	133	121	88	153
	6	89	102	86	109	91	75	91	81	83	77

Table 8

Table 8. $CCR2^{+}$ cells scoring in immunohistochemistry.

Group	Animal No.	ROI 1	ROI 2	ROI 3	ROI 4	ROI 5	ROI 6	ROI 7	ROI 8	ROI 9	ROI 10
Normal	1	13	38	13	17	21	28	4	5	6	10
	2	14	44	36	13	10	33	25	17	4	17
	3	4	10	11	8	39	26	19	4	2	5
	4	2	8	1	9	5	4	3	4	15	6
	5	4	4	12	3	9	3	2	3	12	14
	6	6	10	5	39	3	24	7	12	3	3
5 weeks	1	16	25	16	11	26	7	8	21	26	16
	2	11	8	20	15	20	6	13	18	46	12
	3	27	12	10	16	23	7	13	23	12	16
	4	20	11	10	19	38	7	12	8	28	9
	5	20	15	15	9	17	14	30	25	24	9
	6	21	23	16	44	71	13	15	17	13	37
6 weeks	1	12	27	55	26	44	160	44	26	70	32
	2	43	14	33	17	19	19	54	22	17	16
	3	19	36	45	82	58	41	35	48	31	19
	4	18	35	56	12	29	15	20	44	25	30
	5	98	19	21	25	35	24	38	35	24	92
7 weeks	1	52	75	58	32	58	32	47	45	46	53
	2	52	33	58	30	35	19	42	36	32	46
	3	37	52	49	36	40	44	30	25	25	55
	4	65	81	54	80	63	63	68	60	64	47
	5	42	34	35	33	45	70	47	53	43	41
	6	40	47	42	29	44	31	36	22	54	47

Table 9

Table 9. $CD163^+$ cells scoring in immunohistochemistry.

Group	Animal No.	ROI 1	ROI 2	ROI 3	ROI 4	ROI 5	ROI 6	ROI 7	ROI 8	ROI 9	ROI 10
Normal	1	213	226	290	232	273	264	203	220	296	236
	2	241	290	269	259	231	245	260	272	234	262
	3	235	234	216	225	241	175	155	177	187	204
	4	153	179	160	185	187	185	213	231	202	173
	5	199	207	239	226	249	207	229	250	226	234
	6	243	240	270	212	243	242	268	222	195	199
5 weeks	1	229	112	137	167	92	91	108	74	109	79
	2	132	197	100	110	131	108	155	123	152	204
	3	258	179	124	145	248	209	129	149	187	161
	4	119	105	112	183	109	178	100	150	119	183
	5	190	103	83	90	107	137	124	98	128	109
	6	105	136	82	104	80	107	194	137	95	118
6 weeks	1	210	173	247	169	230	121	366	103	119	130
	2	294	95	120	185	155	237	255	107	246	187
	3	180	121	107	156	175	81	132	149	102	160
	4	253	138	157	108	123	166	119	195	135	100
	5	224	147	185	126	107	150	118	108	104	130
7 weeks	1	266	138	152	175	235	129	200	146	155	177
	2	181	193	150	187	210	154	192	115	158	164
	3	341	164	183	165	151	155	158	134	144	139
	4	235	179	224	306	198	144	147	128	160	124
	5	100	182	156	164	176	220	211	156	147	280
	6	173	207	152	168	172	154	142	180	150	145

Table 10

Table 10. $CD4^+$ cells scoring in immunohistochemistry.

Group	Animal No.	ROI 1	ROI 2	ROI 3	ROI 4	ROI 5	ROI 6	ROI 7	ROI 8	ROI 9	ROI 10
Normal	1	20	6	9	15	9	7	8	10	9	10
	2	27	16	12	13	16	13	22	23	14	12
	3	6	6	9	10	6	8	13	9	5	9
	4	8	4	10	4	6	6	9	5	6	4
	5	4	3	4	4	7	5	4	3	4	6
	6	6	5	8	7	5	9	6	7	6	8
5 weeks	1	12	10	12	14	7	11	14	8	11	7
	2	16	18	23	24	27	21	16	13	16	9
	3	16	13	13	10	13	14	11	8	11	11
	4	18	17	16	24	20	33	18	14	21	18
	5	16	14	16	13	24	19	14	13	15	16
	6	13	3	9	9	10	10	13	11	13	7
6 weeks	1	30	16	20	22	24	20	18	24	17	13
	2	14	14	14	8	16	9	13	17	10	8
	3	19	17	11	10	18	11	9	10	13	10
	4	12	9	9	10	12	7	13	6	19	11
	5	11	17	15	8	7	13	9	13	11	11
7 weeks	1	22	9	15	11	12	12	9	14	13	12
	2	12	15	9	7	7	6	14	7	14	14
	3	10	10	13	12	12	15	18	16	13	15
	4	18	18	17	23	14	13	26	13	25	16
	5	15	22	10	9	18	12	6	8	7	14
	6	13	12	12	13	13	13	20	20	8	12

Table 11

Table 11. $CD8^+$ cells scoring in immunohistochemistry.

Group	Animal No.	ROI 1	ROI 2	ROI 3	ROI 4	ROI 5	ROI 6	ROI 7	ROI 8	ROI 9	ROI 10
Normal	1	6	8	6	6	5	5	7	6	6	5
	2	24	23	19	26	30	20	22	18	17	27
	3	6	6	6	6	2	4	6	5	4	3
	4	3	6	5	4	9	5	7	7	6	7
	5	5	7	10	5	13	7	10	5	7	6
	6	5	6	4	4	7	5	4	5	3	3
5 weeks	1	9	15	13	6	15	14	23	14	12	7
	2	21	18	9	9	17	17	19	16	12	7
	3	6	13	14	9	8	13	13	6	16	16
	4	17	7	15	16	9	11	17	22	52	21
	5	22	23	21	14	15	39	17	24	20	14
	6	12	8	9	11	13	19	20	10	5	8
6 weeks	1	33	20	18	12	23	18	14	35	8	26
	2	8	12	11	7	19	8	11	9	7	8
	3	24	15	10	19	18	13	26	10	9	9
	4	8	10	10	7	7	6	13	21	5	4
	5	8	14	11	7	6	7	16	7	12	18
7 weeks	1	17	7	16	13	12	21	8	11	14	20
	2	14	13	15	20	12	22	36	26	14	12
	3	10	13	11	13	13	16	14	24	19	9
	4	39	24	28	34	41	54	16	31	83	37
	5	41	23	33	16	17	16	13	19	23	21
	6	15	17	15	9	15	14	18	9	28	14

Table 12

Table 12. Individual data on the proportion of hepatic immune cells analyzed based on the gating strategy in Flow cytometry (%).

Group	Animal No.	$CD3^{hi}$	$CD3^{hi}$ $CD4^{hi}$	$CD3^{hi}$ $CD8^{hi}$	$F4/80^{hi}$	$F4/80^{hi}$ $CD11b^{hi}$ $Ly\text{-}6c^{hi}$	$F4/80^{hi}$ $CD11b^{low}$ $Ly\text{-}6c^{low}$
Normal	1	19.4	43.6	24	12	53.1	12.4
	2	34.6	29.3	52.5	13.6	52.4	5.36
	3	20.7	36.3	26.5	14.3	50	13.8
	4	18.7	35	29.9	13.8	45	17
	5	18.4	37.9	29.6	11.6	46.3	13.9
	6	20.4	42.7	27	8.94	39.2	9.05
5 weeks	1	20.4	34.9	39.6	10.8	68.6	8.95
	2	21.8	31.3	40.3	12	65.1	9.64
	3	17.9	33.6	42.6	13.2	60.9	7.93
	4	19.2	30.7	49.2	10.9	64	12.4
	5	21.9	22.9	46.3	5.97	62	0.085
	6	21	28.4	38.1	8.22	56.2	0.068
6 weeks	1	39.6	24.1	56.4	19.9	67.4	11.7
	2	24.7	27.6	36.4	17.4	57	19.3
	3	28.4	30.6	43.3	20.8	57.3	12.4
	4	24.4	37.2	34.4	19.9	55.3	14.5
	5	29.1	37.4	41.9	20.4	64.5	9.79
7 weeks	1	33	40.4	44.5	-	-	-
	2	34.4	39	45.4	-	-	-
	3	25.8	44.5	40.1	-	-	-
	4	31	32.5	51.3	-	-	-
	5	24.5	30.4	51.6	-	-	-
	6	26.9	33.6	50.2	-	-	-

REFERENCES

1. Younossi ZM, Koenig AB, Abdelatif D, Fazel Y, Henry L, Wymer M. Global epidemiology of nonalcoholic fatty liver disease—meta analytic assessment of prevalence, incidence, and outcomes. Hepatology. 2016;64(1):73-84.

2. Anstee QM, Reeves HL, Kotsiliti E, Govaere O, Heikenwalder M. From NASH to HCC: current concepts and future challenges. Nature reviews Gastroenterology & hepatology. 2019;16(7):411-28.

3. Younossi Z, Anstee QM, Marietti M, Hardy T, Henry L, Eslam M, et al. Global burden of NAFLD and NASH: trends, predictions, risk factors and prevention. Nature reviews Gastroenterology & hepatology. 2018;15(1):11-20.

4. Lazo M, Clark JM, editors. The epidemiology of nonalcoholic fatty liver disease: a global perspective. Seminars in liver disease; 2008: © Thieme Medical Publishers.

5. Serfaty L, Lemoine M. Definition and natural history of metabolic steatosis: clinical aspects of NAFLD, NASH and cirrhosis. Diabetes & metabolism. 2008;34(6):634-7.

6. Streba LAM, Vere CC, Rogoveanu I, Streba CT. Nonalcoholic fatty liver disease, metabolic risk factors, and hepatocellular carcinoma: an open question. World journal of gastroenterology: WJG. 2015;21(14):4103.

7. Park JH, Koo BK, Kim W, Kim W-H. Histological severity of nonalcoholic fatty liver disease is associated with 10-year risk for atherosclerotic cardiovascular disease. Hepatology International. 2021:1-12.

8. Narayanan S, Surette FA, Hahn YS. The immune landscape in nonalcoholic steatohepatitis. Immune Network. 2016;16(3):147.

9. Ioannou GN. The role of cholesterol in the pathogenesis of NASH. Trends in Endocrinology & Metabolism. 2016;27(2):84-95.

10. Farrell G, Schattenberg JM, Leclercq I, Yeh MM, Goldin R, Teoh N, et al. Mouse models of nonalcoholic steatohepatitis: toward optimization of their relevance to human nonalcoholic steatohepatitis. Hepatology. 2019;69(5):2241-57.

11. Ascha MS, Hanouneh IA, Lopez R, Tamimi TAR, Feldstein AF, Zein NN. The incidence and risk factors of hepatocellular carcinoma in patients with nonalcoholic steatohepatitis. Hepatology. 2010;51(6):1972-8.

12. Meli R, Mattace Raso G, Calignano A. Role of innate immune response in non-alcoholic fatty liver disease: metabolic complications and therapeutic tools. Frontiers in immunology. 2014;5:177.

13. Ganz M, Bukong TN, Csak T, Saha B, Park J-K, Ambade A, et al. Progression of non-alcoholic steatosis to steatohepatitis and fibrosis parallels cumulative accumulation of danger signals that promote inflammation and liver tumors in a high fat–cholesterol–sugar diet model in mice. Journal of translational medicine. 2015;13(1):1-14.

14. Peng C, Stewart AG, Woodman OL, Ritchie RH, Qin CX. Non-alcoholic steatohepatitis: A review of its mechanism, models and medical treatments. Frontiers in Pharmacology. 2020;11:1864.

15. Brown ZJ, Heinrich B, Greten TF. Mouse models of hepatocellular carcinoma: an overview and highlights for immunotherapy research. Nature reviews Gastroenterology & hepatology. 2018;15(9):536-54.

16. Leenders MW, Nijkamp MW, Rinkes IHB. Mouse models in liver cancer research: a review of current literature. World journal of gastroenterology: WJG. 2008;14(45):6915.

17. Bakiri L, Wagner EF. Mouse models for liver cancer. Molecular oncology. 2013;7(2):206-23.

18. Ray RB, Lagging LM, Meyer K, Ray R. Hepatitis C virus core protein cooperates with ras and transforms primary rat embryo fibroblasts to tumorigenic phenotype. Journal of Virology. 1996;70(7):4438-43.

19. Sandgren E, Quaife CJ, Pinkert CA, Palmiter RD, Brinster RL. Oncogene-induced liver neoplasia in transgenic mice. Oncogene. 1989;4(6):715-24.

20. Calvisi DF, Wang C, Ho C, Ladu S, Lee SA, Mattu S, et al. Increased lipogenesis, induced by AKT-mTORC1-RPS6 signaling, promotes development of human hepatocellular carcinoma. Gastroenterology. 2011;140(3):1071-83. e5.

21. Agosti P, Sabbà C, Mazzocca A. Emerging metabolic risk factors in hepatocellular carcinoma and their influence on the liver microenvironment. Biochimica et Biophysica Acta (BBA)-Molecular Basis of Disease. 2018;1864(2):607-17.

22. Capece D, Fischietti M, Verzella D, Gaggiano A, Cicciarelli G, Tessitore A, et al. The inflammatory microenvironment in hepatocellular carcinoma: a pivotal role for tumor-associated macrophages. BioMed research international. 2013;2013.

23. Hernandez–Gea V, Toffanin S, Friedman SL, Llovet JM. Role of the microenvironment in the pathogenesis and treatment of hepatocellular carcinoma. Gastroenterology. 2013;144(3):512-27.

24. Reid D, Reyes J, McDonald B, Vo T, Reimer R, Eksteen B. Kupffer cells undergo fundamental changes during the development of experimental NASH and are critical in initiating liver damage and inflammation. PloS one. 2016;11(7):e0159524.

25. Pfister D, Núñez NG, Pinyol R, Govaere O, Pinter M, Szydlowska M, et al. NASH limits anti-tumour surveillance in immunotherapy-treated HCC. Nature. 2021;592(7854):450-6.

26. Orime K, Shirakawa J, Togashi Y, Tajima K, Inoue H, Nagashima Y, et al. Lipid-lowering agents inhibit hepatic steatosis in a non-alcoholic steatohepatitis-derived hepatocellular carcinoma mouse model. European journal of pharmacology. 2016;772:22-32.

27. Middleton SA, Rajpal N, Cutler L, Mander P, Rioja I, Prinjha RK, et al. BET inhibition improves NASH and liver fibrosis. Scientific reports. 2018;8(1):1-13.

28. Fujii M, Shibazaki Y, Wakamatsu K, Honda Y, Kawauchi Y, Suzuki K, et al. A murine

model for non-alcoholic steatohepatitis showing evidence of association between diabetes and hepatocellular carcinoma. Medical molecular morphology. 2013;46(3):141-52.

29. Takakura K, Koido S, Fujii M, Hashiguchi T, Shibazaki Y, Yoneyama H, et al. Characterization of non-alcoholic steatohepatitis-derived hepatocellular carcinoma as a human stratification model in mice. Anticancer research. 2014;34(9):4849-55.

30. Van Herck MA, Weyler J, Kwanten WJ, Dirinck EL, De Winter BY, Francque SM, et al. The differential roles of T cells in non-alcoholic fatty liver disease and obesity. Frontiers in immunology. 2019;10:82.

31. Hashimoto D, Chow A, Noizat C, Teo P, Beasley MB, Leboeuf M, et al. Tissue-resident macrophages self-maintain locally throughout adult life with minimal contribution from circulating monocytes. Immunity. 2013;38(4):792-804.

32. Zigmond E, Samia-Grinberg S, Pasmanik-Chor M, Brazowski E, Shibolet O, Halpern Z, et al. Infiltrating monocyte-derived macrophages and resident kupffer cells display different ontogeny and functions in acute liver injury. The Journal of Immunology. 2014;193(1):344-53.

33. Murray PJ, Wynn TA. Protective and pathogenic functions of macrophage subsets. Nature reviews immunology. 2011;11(11):723-37.

34. Jindal A, Bruzzì S, Sutti S, Locatelli I, Bozzola C, Paternostro C, et al. Fat-laden macrophages modulate lobular inflammation in nonalcoholic steatohepatitis (NASH). Experimental and molecular pathology. 2015;99(1):155-62.

35. Karlmark KR, Weiskirchen R, Zimmermann HW, Gassler N, Ginhoux F, Weber C, et al. Hepatic recruitment of the inflammatory Gr1+ monocyte subset upon liver injury promotes hepatic fibrosis. Hepatology. 2009;50(1):261-74.

36. Antoniades CG, Quaglia A, Taams LS, Mitry RR, Hussain M, Abeles R, et al. Source and characterization of hepatic macrophages in acetaminophen induced acute liver failure in humans. Hepatology. 2012;56(2):735-46.

37. Holt MP, Cheng L, Ju C. Identification and characterization of infiltrating macrophages in acetaminophen induced liver injury. Journal of leukocyte biology. 2008;84(6):1410-21.

38. Heymann F, Hammerich L, Storch D, Bartneck M, Huss S, Rüsseler V, et al. Hepatic macrophage migration and differentiation critical for liver fibrosis is mediated by the chemokine receptor C C motif chemokine receptor 8 in mice. Hepatology. 2012;55(3):898-909.

39. Ramachandran P, Pellicoro A, Vernon MA, Boulter L, Aucott RL, Ali A, et al. Differential Ly-6C expression identifies the recruited macrophage phenotype, which orchestrates the regression of murine liver fibrosis. Proceedings of the National Academy of Sciences. 2012;109(46):E3186-E95.

40. Dambach DM, Watson LM, Gray KR, Durham SK, Laskin DL. Role of CCR2 in macrophage migration into the liver during acetaminophen-induced hepatotoxicity in the mouse. Hepatology. 2002;35(5):1093-103.

41. Jenkins SJ, Ruckerl D, Cook PC, Jones LH, Finkelman FD, Van Rooijen N, et al. Local macrophage proliferation, rather than recruitment from the blood, is a signature of TH2 inflammation. science. 2011;332(6035):1284-8.

42. Zigmond E, Varol C, Farache J, Elmaliah E, Satpathy AT, Friedlander G, et al. Ly6Chi monocytes in the inflamed colon give rise to proinflammatory effector cells and migratory antigen-presenting cells. Immunity. 2012;37(6):1076-90.

43. Davies LC, Rosas M, Jenkins SJ, Liao C-T, Scurr MJ, Brombacher F, et al. Distinct bone marrow-derived and tissue-resident macrophage lineages proliferate at key stages during inflammation. Nature communications. 2013;4(1):1-10.

44. Yan C, Yang Q, Gong Z. Tumor-associated neutrophils and macrophages promote gender disparity in hepatocellular carcinoma in zebrafish. Cancer research. 2017;77(6):1395-407.

45. de Oliveira S, Houseright RA, Graves AL, Golenberg N, Korte BG, Miskolci V, et al. Metformin modulates innate immune-mediated inflammation and early progression of NAFLD-associated hepatocellular carcinoma in zebrafish. Journal of hepatology. 2019;70(4):710-21.

46. Kleiner DE, Brunt EM, Van Natta M, Behling C, Contos MJ, Cummings OW, et al. Design and validation of a histological scoring system for nonalcoholic fatty liver disease. Hepatology. 2005;41(6):1313-21.

47. Sun D, Luo T, Dong P, Zhang N, Chen J, Zhang S, et al. CD86+/CD206+ tumor-associated macrophages predict prognosis of patients with intrahepatic cholangiocarcinoma. PeerJ. 2020;8:e8458.

48. Breuer DA, Pacheco MC, Washington MK, Montgomery SA, Hasty AH, Kennedy AJ. CD8+ T cells regulate liver injury in obesity-related nonalcoholic fatty liver disease. American Journal of Physiology-Gastrointestinal and Liver Physiology. 2020;318(2):G211-G24.

49. Krenkel O, Puengel T, Govaere O, Abdallah AT, Mossanen JC, Kohlhepp M, et al. Therapeutic inhibition of inflammatory monocyte recruitment reduces steatohepatitis and liver fibrosis. Hepatology. 2018;67(4):1270-83.

국문요약

비알코올성 지방간염 동물 모델을 이용한 간 조직의 면역 미세환경 분석

비알코올성 지방간염은 전세계적으로 유병률이 증가하는 추세이며 간세포암종으로 진전될 수 있는 위험한 질환이지만, 이를 치료하기 위해 승인된 약물은 없다. 이에 따라 비알코올성 지방간염에 대한 연구가 활발하게 진행되고 있고 특히 간 조직 내 미세환경의 변화가 질병의 진전에 어떻게 영향을 미치는지에 대한 연구의 필요성이 증대되고 있다.

본 연구에서는 Stelic animal model (STAM)을 이용하여 비알코올성 지방간염 초기 단계에서 간 조직 내 면역 미세환경의 변화에 주목하여 간에 상주하는 면역세포와 외부에서 침윤해온 면역세포의 거동을 관찰하였다. 정상 상태와 비교했을 때 비알코올성 지방간이 진전될수록 혈액을 통해 순환 중이던 단핵구 기원의 대식세포의 활동이 두드러짐을 확인하였다. 이와 함께 질병상태에서 간 내 M2 대식세포가 차지하는 비율이 감소해 있음을 관찰하였다. 이는 정상 상태에서의 M1/M2 대식세포의 균형이 깨졌음을 간접적으로 유추할 수 있는 정보였다. 또한, 질병이 진전될수록 도움 T 세포보다는 세포독성 T 세포의 활성이 두드러짐을 확인하였다.

STAM 모델은 단기간에 비알코올성 지방간부터 간세포암종까지 유도가 되고 사람에서의 임상적 기준(clinical stratification)을 반영할 수 있는 좋은 동물모델이다. 기존 연구에서는 식이요법, 화학요법 등을 통해 비알코올성 지방간을

유도하여 많은 연구 결과들을 제시하였지만 이 모델들은 짧은 시간 내에 간세포암종까지 유도가 어려우며 사람과의 유사성이 떨어진다는 한계가 존재한다. 이에 본 연구에서는 임상적 기준과 가장 유사하다고 판단되는 STAM 모델에서 유세포분석법과 면역조직화학염색 기법을 이용하여 간 내 미세환경의 변화를 처음 관찰하였고, 이는 후속 연구 진행에 중요한 기반이 될 것으로 기대한다.

중심단어: non-alcoholic fatty liver disease (NAFLD), non-alcoholic steatohepatitis (NASH), hepatocellular carcinoma (HCC), stelic animal model (STAM), Kupffer cell (KC), monocyte-derived macrophage (MoMF)